AD NUMBER
AD441930
LIMITATION CHANGES
TO: **Approved for public release; distribution is unlimited. Document partially illegible.**
FROM: **Distribution authorized to U.S. Gov't. agencies and their contractors; Administrative/Operational Use; JUN 1964. Other requests shall be referred to Army Missile Command, Redstone Arsenal, AL.**
AUTHORITY
rsic ltr, 20 sep 1965

GDA-DBE64-034
Space Science Laboratory

RE-ENTRY PHYSICS RESEARCH

SEMI-ANNUAL REPORT

UNITED STATES ARMY MISSILE COMMAND

CONTRACT DA-04-495-ORD-3383(Z),
AMENDMENT NO. 15
ARPA ORDER NO. 393, AMENDMENT NO. 2

JUNE 1964

This research is a part of Project DEFENDER,
sponsored by the
Advanced Research Projects Agency,

Department of Defense

GENERAL DYNAMICS | ASTRONAUTICS

ADDENDA

Legend to Fig. VII-1

(a) Schematic of optical system for wake reversal temperature measurement.

S - source, American Optical Model 2434 DC carbon arc

L_1, L_2, L_3 - plano-convex doublet lens sets with 3.75" effective chamber and 6" effective focal length, one- to- one imaging

KCF - Kerr Cell Filter

P_1, P_2 - Polaroid HN-38 polarizers

KC - Electro-Optical Instruments, Inc. Model K60/90PL Kerr cell

W_1, W_2 - test section windows with effective 5.25" diameter

LM - lens mask to restrict collect solid angle of radiation from wake to that of the source, 3" diameter

M - Perkin-Elmer Model 98-G grating monochromator with 1800 lines/mm grating blazed for 5000 Å in first order

BS - beam splitter at monochromator exit plane

$PM(\lambda_1)$,

$PM(\lambda_2)$ - RCA 7265 14 stage, S-20 response, photomultipliers monitoring radiation at 5890 Å (λ_1) and 5880 Å (λ_2)

All lenses and windows have been over-coated with magnesium fluoride to reduce reflection losses.

(b) Schematic of beam splitter used to separate wavelength intervals.

GDA-DBE64-034
Space Science Laboratory

RE-ENTRY PHYSICS RESEARCH

SEMI-ANNUAL REPORT

UNITED STATES ARMY MISSILE COMMAND

CONTRACT DA-04-495-ORD-3383(Z);
AMENDMENT NO. 15
ARPA ORDER NO. 393, AMENDMENT NO. 2

JUNE 1964

This research is a part of Project DEFENDER,
sponsored by the
Advanced Research Projects Agency,

Department of Defense.

TABLE OF CONTENTS

INTRODUCTION 1

3" SHOCK TUBE PROGRAM SUMMARY 2

I. INDUCTION PERIOD PRECEDING CO_2-FORMATION IN SHOCK HEATED CO-O_2-AR MIXTURES 5

II. INFLUENCE OF H_2 ON THE INDUCTION PERIOD PRECEDING CO_2-FORMATION IN SHOCK HEATED CO-O_2-Ar-MIXTURES 17

III. REVIEW OF LITERATURE ON CO-OXIDATION 18

IV. COMPUTER CODE FOR CHEMICALLY REACTING, SHOCK HEATED MIXTURES 20

V. MICROWAVE WAKE INTERACTION STUDIES 21

VI. FLUID DYNAMICS 25

VII. HYPERVELOCITY WAKE TEMPERATURE MEASUREMENTS 49

VIII. 6 MM LIGHT GAS GUN RANGE 58

IX. 24" SHOCK TUBE 61

INTRODUCTION

This report describes the re-entry physics research activities at General Dynamics/Astronautics during the approximate time interval of December 1963 through May 1964 under Contract DA-04-495-ORD-3383(Z), Amendment No. 15, ARPA Order No. 393, Amendment No. 2. The individual research topics studied under this contract are separately discussed in the following sections, including a description of two new facilities, developed under General Dynamics/Astronautics funding, to be used in the second half of the contract year.

3" SHOCK TUBE PROGRAM SUMMARY - K. C. P. Saltzman

During the first six months of the contract period experimental shock tube studies of the induction period preceding the onset of measurable CO_2-formation in argon diluted mixtures of CO and O_2 with less than 1 ppm hydrogen contamination have been completed.

The measurements were conducted at temperatures between 1500 and 3000°K and at total pressure between 0.5 and 1.5 atm. The empirical results of these measurements are that over the range of temperatures, pressures and initial concentrations employed the induction period is (a) independent of the vibrational relaxation of CO, O_2 and CO_2, (b) inversely proportional to the square root of the mole concentrations of CO and O_2, and (c) related to an apparent activation energy which changes from about 21 kcal/mole at $1500^{\circ}K \leq T \leq 2000^{\circ}K$ to about 34 kcal/mole at $2500^{\circ}K \leq T \leq 3000^{\circ}K$. The details of these investigations are presented in Section I below.

In the course of these studies it was found that addition of 0.1% H_2 to the reacting mixture does not only result in a decrease of the induction period as expected but also results in a constant apparent activation energy of about 21 kcal/mole over the total range of temperatures between 1500 and 3000°K. From this observation it has been concluded that in the presence of hydrogen below a certain temperature, depending on the amount of hydrogen present, different chemical reactions may become responsible than those governing the induction process in mixtures with about 1 ppm hydrogen above 2500°K.

Measurements of the induction period as a function of temperature and the initial concentrations of H_2, CO and O_2 have been started and partially

completed (Section II). These investigations will be continued in order to determine the important reaction steps responsible for CO_2-formation in the presence of hydrogen. Furthermore, some induction period data have been obtained with N_2 replacing the Ar-diluent, in order to study the influence of the diluent gas on the induction time.

The literature search, mentioned in the last annual report, for kinetic data on the reactions occurring in CO/O_2 systems has been extended and a critical review of the information obtained has been completed (Section III). Although no literature information is available at the present time about the pertinent chemical reactions governing the induction of CO_2 formation in $CO/O_2/H_2$ systems, these studies provided and will provide in the future valuable guide lines for the construction of reasonable reaction schemes and for the definition of critical experiments. Furthermore, from these studies it became apparent that the bulk of the luminosity between 2500 and 5500Å in reacting $CO/O_2/H_2$ systems may be accounted for by the chemiluminescent CO-flame band emission under re-entry conditions. The energy emitted in this spectral region is proportional to the mole concentrations of carbon monoxide and atomic oxygen and can be calculated within a factor of 10 for known temperature and concentrations of CO and O (Section III).

The computer code for chemically reacting, shock heated gases which we have received without cost from Cornell Aeronautical Laboratory, Inc. has been adapted for our 7094-computer (Section IV). Test runs with this code will be conducted in the immediate future. The code is intended to be used in the analysis of chemical reaction schemes relevant to the interpretation of the shock tube studies of CO_2-formation. It can also be used for computations of reaction time histories in inviscid flow models without diffusion pertaining to wakes.

Dr. E. F. Myers, Jr. and Mr. K. C. P. Sulzmann attended the Symposium on Chemical Reactions in Shock Tubes at the U. S. Army Research Office-Dunham, Durham, North Carolina, April 20-22, 1954, where Mr. Sulzmann presented a paper on Shock Tube Studies of CO_2 Formation.

I. INDUCTION PERIOD PRECEDING CO_2-FORMATION IN SHOCK HEATED CO-O_2-Ar MIXTURES[1] - K. G. P. Sulzmann, B. F. Myers, Jr., E. R. Bartle

The clarification of the chemical kinetics governing the formation of CO_2 in mixtures of CO and O_2 requires studies of the time history of the reaction process. Empirical results are presented of studies of the time resolved initial behavior of the CO-O_2 system with argon diluent as a heat bath by shock tube techniques under conditions for which the oxidation reactions of CO are sustained by the shock wave. The oxidation history of CO was studied at temperatures between 1500 and 3000°K and at total pressures between 0.5 and 1.5 atm by spectroscopical techniques employing spectral portions of the CO-fundamental and CO_2-ν_3-fundamental infrared bands as well as spectral portions of the CO-flame "continuum" emission. These techniques led to the observation of an induction period preceding the onset of measurable electronic ground state CO_2-formation and quantitative information about the dependence of the induction period on the initial mole concentrations of CO and O_2, the total gas pressure and the temperature.

The measurements were conducted behind incident shock waves traveling through argon diluted mixtures of CO and O_2. The pressure driven shock tube, the gas handling and mixing procedure, as well as the spectroscopic techniques employed have been described previously in detail.[2] In particular, the time histories of three radiation parameters have been registered simultaneously: (a) the infrared emission of and transmission through CO_2 at 4.25μ (spectral interval: $\Delta\lambda$ = 0.043μ), (b) the infrared emission of CO at 5.07μ ($\Delta\lambda$ = 0.130μ), and (c) the CO-flame "continuum" emission at 4457Å ($\Delta\lambda$ = 40Å) and at 3064Å ($\Delta\lambda$ = 7Å).

The intermittent CO_2-emission-transmission measurements have been used to obtain information about the time history of the CO_2-formation behind the shock wave. The intermittent measurement was accomplished by chopping mechanically the light beam of the transmitting light source with a chopper wheel at about 10^5 cps before its passage through the shock tube. At the same time the CO-emission has been utilized to obtain additional information about the CO vibrational relaxation and the consumption of CO during the early time history of the chemical interaction between CO and O_2. For these measurements liquid nitrogen cooled In-Sb-photovoltaic detectors have been used. The detector-amplifier circuits had rise times of less than 0.1 μsec. Furthermore, the CO-flame "continuum" was used as an indicator for the onset of measurable atomic oxygen production; the origin of this radiation is essentially related[3,4] to the overall radiative recombination process $CO + O \rightarrow CO_2 + h\nu$. The radiation observed in the chosen spectral interval at 3064Å includes the band heads of the OH(0-0) electronic band and the CO-flame "continuum" which extends approximately from 2500 to 6000Å. The photomultiplier-amplifier circuits used[1] had rise times of less than 1 μsec.

The test gas mixtures were prepared from Matheson C.P. grade supplies of CO, O_2, and Ar. The supply gases were first condensed in a separate cold trap at the temperature of liquid nitrogen. Portions of the condensed gases were distilled off before the remaining condensates were distilled into an evacuated (2×10^{-5} mm Hg) glass lined 80 liter mixing tank. The total pressure of the prepared gas mixtures was about 1 atm so that contamination of the mixtures by H_2O, if present, was less than 0.1 ppm. The overall hydrogen contamination of the final test gas mixtures after admission into the shock tube was between 0.5 and 1 ppm as determined by mass spectro-

metric analysis with an Aero-Vac vacuum analyzer.

The following mole percentages of O_2, CO and Ar have been used in order to determine the dependence on initial concentration, total pressure and temperature of the induction period:

Mixture A_1: 9.98% O_2 + 20.03% CO + 69.99% Ar

B_1: 5.00% O_2 + 10.00% CO + 85.00% Ar

C_1: 9.99% O_2 + 10.01% CO + 80.00% Ar

D : 20.00% O_2 + 10.00% CO + 70.00% Ar.

Furthermore, in order to study the effects of the vibrational relaxation of the reactant molecules CO and O_2 on the induction period the vibrational relaxation rates of CO and O_2 were increased by adding or substituting for argon up to 5% He in the above mixtures:

Mixture A_2: 9.51% O_2 + 19.08% CO + 66.65% Ar + 4.76% He

B_2: 5.01% O_2 + 10.13% CO + 79.88% Ar + 4.98% He

C_2: 10.02% O_2 + 9.98% CO + 75.01% Ar + 4.99% He

C_3: 9.51% O_2 + 9.53% CO + 76.18% Ar + 4.78% He.

The initial thermodynamic state of the individual test gas mixtures behind the incident shock wave was calculated from the gas state in front of the shock wave and the shock velocity using one-dimensional normal shock theory under the assumption of equilibration of the internal degrees of freedom and frozen chemical reactions. Shock velocity measurements in argon along three sections of the shock tube resulted in deviations of at most - 0.5% from the shock velocities obtained with the reacting mixtures under equivalent operating conditions; attenuation of the shock propagation was observed in all mixtures used, and, within the experimental scatter, no differences in shock propagation were detected between the different reacting mixtures. The shock parameter calculations were performed on a 7090-IBM

computer with the Los Alamos GMX-7 shock parameter code.* This code requires polynomial fits for the enthalpy and the free energy of the chemical species which were obtained from the compilation of high temperature thermodynamic data as given by Hochstim.[5] The representation of the data in terms of a computed temperature T_i for fully equilibrated internal degrees of freedom and frozen chemistry has been chosen for the sake of convenience. This procedure introduces a maximum systematic temperature error of less than - 3% and a maximum systematic error in the normalized induction and vibrational relaxation data of less than - 8% when compared with calculations based upon frozen internal degrees of freedom.

The main result of the CO_2-formation studies is the observation of an induction period preceding the formation of measurable amounts of electronic ground state CO_2 molecules and the onset of CO-flame "continuum" emission behind the shock wave. Within the experimental accuracy, no difference between the induction period for the onset of CO_2-formation and the induction period for the onset of "continuum" emission was observed.

For purposes of quantitative comparison an induction time τ_i^L (laboratory time) was defined by taking the intercept of the tangent to the CO_2-emission signal at the observed inflection point (steepest slope) with the horizontal line corresponding to the zero level signal before shock arrival. The induction time τ_i^L was converted into an induction period parameter α_i^o by multiplication with both, the density ratio ρ_i/ρ_o across the shock front and the total pressure P_i, viz.:

$$\alpha_i^o = \tau_i^L \, (\rho_i/\rho_o) \, P_i/\text{atm} \; \mu\text{sec} \; . \qquad (1)$$

It turned out that the linear pressure normalization resulted in the best

---

* Courtesy of Dr. G. L. Schott, Los Alamos Scientific Laboratory, University of California, Los Alamos, New Mexico.

data correlation for the range of pressures P_i between 0.5 and 1.5 atm employed in the measurements.

For the purpose of quantitative comparison of the induction period with the vibrational relaxation of CO, a vibrational "relaxation period" τ_v^L (laboratory time) was defined by the time required for the emission signal I(t) to reach $(1 - e^{-1})$ times its maximum level I_{max}, viz.:

$$I(\tau_v^L)/I_{max} = 1 - e^{-1} = 0.63212 \quad .$$

The "relaxation period" τ_v^L was converted into a vibration rate parameter α_v^o by multiplication with both, the density ratio ρ_i/ρ_o across the shock front and the total pressure P_i, viz.:

$$\alpha_v^o(CO) = \tau_v^L(\rho_i/\rho_o)\ P_i/\text{atm}\ \mu\text{sec} \quad . \qquad (2)$$

The linear pressure normalization of the observed "relaxation periods" resulted in the best data correlation for the range of pressures P_i between 0.5 and 1.5 atm employed in the measurements.

In Figure I-1 a logarithmic plot vs. $1/T_i$ is presented of the data obtained with mixtures C (without and with He added or substituted for Ar) for the induction period parameter, α_i^o, and the vibration rate parameter, $\alpha_v^o(CO)$. In the same figure an estimated upper limit for the O_2-vibration relaxation rate parameter, $\alpha_{v,max}^o(O_2)$, is shown. This estimate is based upon the compilation by Millikan and White[6] of high temperature vibration relaxation data assuming Ar-O_2 and O_2-O_2 translational-vibrational transfer only and assuming the validity of the superposition equation used by these authors for vibrational "relaxation times" of gas mixtures.

At constant temperature, T_i, the induction period parameter, α_i^o, and the vibrational rate parameter, $\alpha_v^o(CO)$, of CO do not show a correlation with the total pressure, P_i, of the individual test runs. Hence, within the

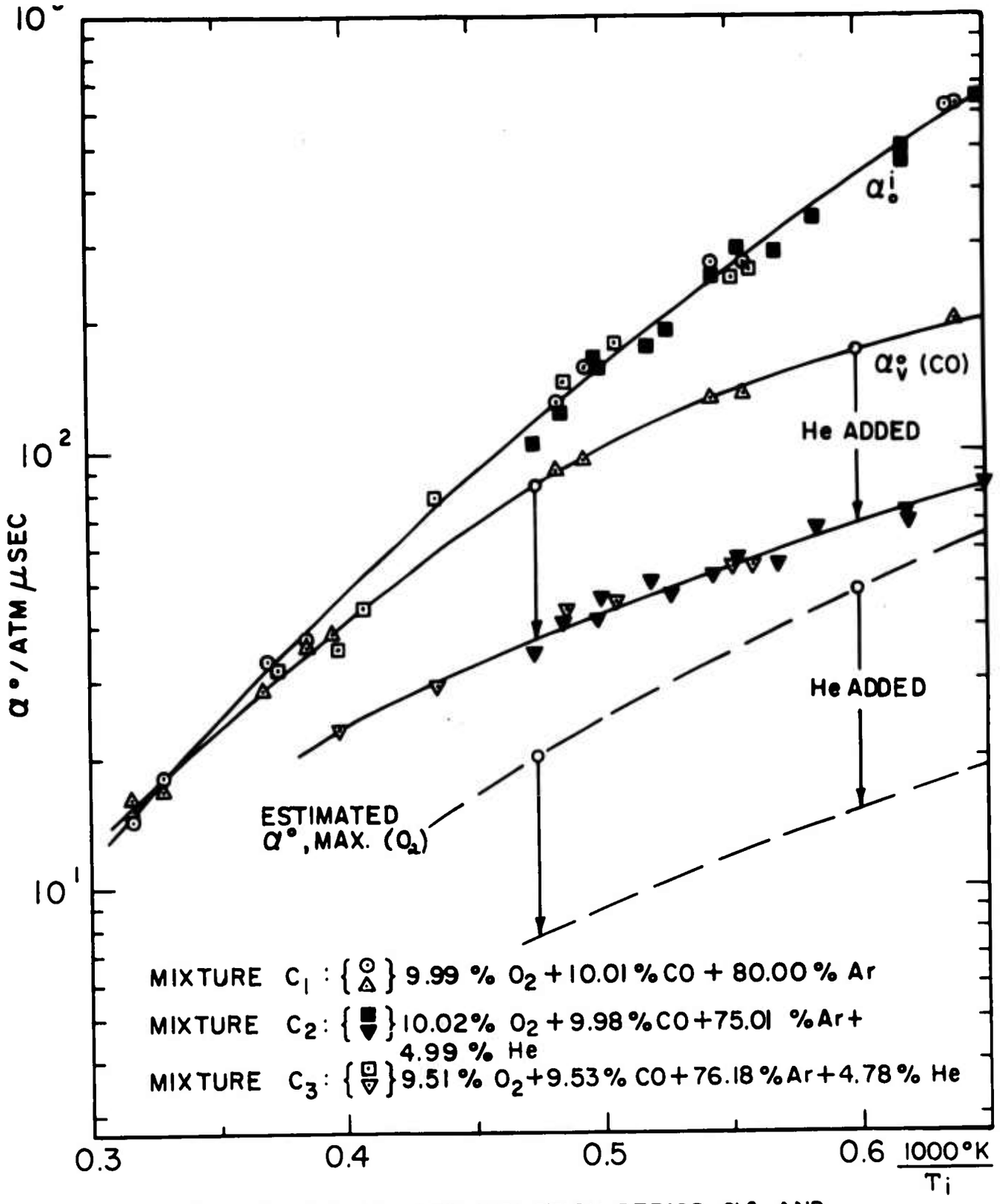

FIG. I-1 : PRESSURE NORMALIZED INDUCTION PERIOD α_i° AND CO-VIBRATION RELAXATION RATE PARAMETER α_v° (CO) VS. $1/T_i$ FOR MIXTURE C. THE DASHED LINES REPRESENT ESTIMATED UPPER LIMITS FOR THE O_2-VIBRATION RELAXATION RATE PARAMETER α_v°, MAX (O_2)

experimental accuracy, these quantities are independent of the total gas pressure and are functions of the temperature, T_i, and the mole fractions of the constituents of the gas mixtures only. This result implies that the induction period, $\tau_i = (\rho_i/\rho_o)\, \tau_i^L$ and the vibrational relaxation period, $\tau_v(CO) = (\rho_i/\rho_o)\, \tau_v^L(CO)$, are inversely proportional to the total gas pressure, P_i.

It is also apparent that the addition (or substitution for argon) of up to 5% helium does not affect the induction period preceding the onset of measurable electronic ground state CO_2-formation; the addition of helium results in a decrease of the vibrational relaxation rate parameter of CO by at least a factor of 2, and of O_2 by at least a factor of 2-1/2. Hence, it may be concluded that the induction period is not directly related to the vibrational relaxation rates of the reactant molecules CO and O_2 nor is it strongly dependent on the change of the vibrational population from a room temperature distribution to distributions at temperatures up to $3000^{\circ}K$. The time required for vibrational equilibration of carbon dioxide[7] is about two orders of magnitude smaller than the induction periods observed in the present measurements; therefore, the effect of vibrational relaxation of the electronic ground state CO_2 on the induction period, if any, is negligible under the present experimental conditions.

Furthermore, it turns out that for the different mixtures used in the experiments the ratios of the induction period parameters are given within the experimental scatter by $\alpha_i^{\circ}(B) : \alpha_i^{\circ}(C) : \alpha_i^{\circ}(A) : \alpha_i^{\circ}(D) = 2 : \sqrt{2} : 1 : 1$ over the range of temperatures employed. From this observation and the mole percentages used it can be implied that the induction period is practically independent of the mole fraction of argon in the mixture and inversely proportional to the square roots of the initial mole fractions x_{CO}° and $x_{O_2}^{\circ}$ of CO

and O_2, viz.:

$$\alpha_i^o = P_i \tau_i = \frac{f(T_i)}{\sqrt{x_{CO}^o x_{O_2}^o}} , \qquad (3)$$

where $f(T_i)$ is a function of the temperature T_i only.

In order to obtain a universal representation of the induction period data as a function of $1/T_i$, an "apparent rate coefficient" $\bar{k}(T_i)$, has been defined by expressing the total pressure, P_i, in equation (3) in terms of the total number of moles, N_i, per cm^3 in the unreacted gas behind the shock front, viz.:

$$\begin{aligned} \bar{k}(T_i) &= \left[\tau_i \sqrt{x_{CO}^o x_{O_2}^o}\, N_i\right]^{-1} \\ &= \left[\tau_i \sqrt{x_{CO}^o x_{O_2}^o}\, (P_i/RT_i)\right]^{-1} \quad ; \end{aligned} \qquad (4)$$

here, R is the universal gas constant and τ_i is the induction period in particle time. The "apparent rate coefficient" has the dimensions of a bimolecular rate coefficient.

In Figure I-2 a universal plot of $\ell n\, \bar{k}^{-1}$ vs. $1/T_i$ is shown for all the induction period data obtained with mixtures A, B, C, and D. The scatter of the data points does not show any correlation with the mole fraction of CO, O_2 and Ar used nor with the total number of moles per unit volume present immediately behind the shock wave in the experiments. Hence, within the experimental accuracy, the "apparent rate coefficient," $\bar{k}$, as defined by equation (4) turns out to be a function of the temperature T_i only over the range of experimental parameters employed. The relative experimental error in $\bar{k}^{-1}$ is caused mainly by the scatter in the measurement of τ_i; this error is at most about 10% at the lower temperature limit and increases to at most about 25% at the upper temperature limit. (The two data points obtained with

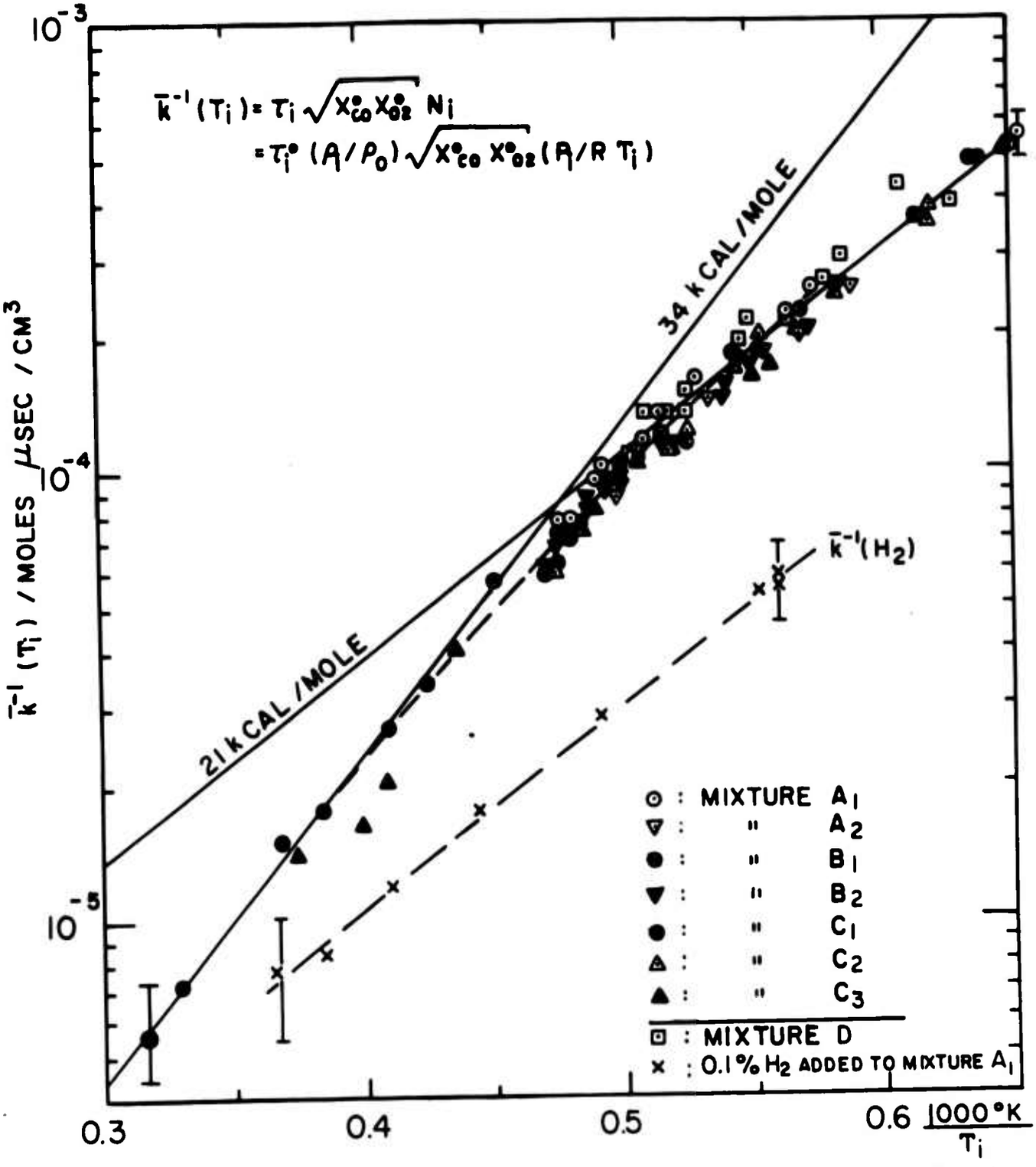

FIG. I-2: UNIFIED PLOT OF INDUCTION PERIOD DATA VS. $1/T_i$ IN TERMS OF AN "APPARENT RATE COEFFICIENT", $\bar{k}$. (THE STRAIGHT LINES REPRESENT LIMITING VALUES OF THE "APPARENT ACTIVATION ENERGY", $E = RT_i \ln(A/\bar{k})$ FOR A = CONST.)

mixture C_3 at about $1000^{\circ}K/T_i = 0.4$ are low because no definite point of inflection was observed within the available time interval of the original oscilloscope traces for the CO_2-emission signal.)

The change in slope of the data for $\bar{k}^{-1}$ as a function of $1/T_i$ in Figure 2 cannot be accounted for by assuming that $\bar{k}$ is a single rate coefficient with a pre-exponential temperature dependence. This observation has to be expected in view of the fact that the induction period τ_i is empirically inversely proportional to the square roots of the initial mole fractions of CO and O_2. The empirically established relation (4) is intended to serve as a basis for future discussions of possible reaction mechanisms governing the initial regime of CO_2-formation; these mechanisms will include besides the initiation reactions also reaction steps which account for the increase of the rate of electronic ground state CO_2-formation subsequent to the induction period. In this connection it is worthwhile to point out that over the range of temperatures employed a change in the relative importance of reaction paths may be anticipated. This change is indicated empirically by the fact that the "apparent activation energy" governing the induction period changes from about 21 kcal/mole at $T_i = 1500^{\circ}K$ to about 34 kcal/mole at $T_i = 3000^{\circ}K$. These limiting "apparent activation energies" for the range of temperatures employed have been determined by ignoring a possible pre-exponential temperature dependence; the slopes corresponding to the limiting values of $\bar{k}^{-1}$ are indicated in Figure 2 by the lines labelled 21 kcal/mole and 34 kcal/mole, respectively.

It is interesting to note that the addition of 0.1% H_2 to mixture A results in values for $\ell n\, \bar{k}^{-1}(H_2)$ which as a function of $1/T_i$ follow a straight line corresponding to an "apparent activation energy" of also about 21 kcal/mole (see Figure 2); at temperatures below $2000^{\circ}K$ the values for $\bar{k}^{-1}(H_2)$ are about

three times smaller than the values for $\bar{k}^{-1}$ obtained with mixtures A, B, C and D. At the present time no definite conclusions can be drawn from the agreement observed below 2000°K between the "apparent activation energies" for $\bar{k}^{-1}(H_2)$ and $\bar{k}^{-1}$; but the observed agreement indicates that reaction mechanisms involving H and OH may have to be considered in an attempt to rationalize the induction period data obtained with mixtures A, B, C and D, although the overall hydrogen contamination level was at most 1 ppm in these mixtures.

No rationalization of the empirically established relationship for the induction period as a function of temperature and initial mole concentrations of CO and O_2 in terms of a plausible reaction scheme is given at the present time; it is felt that more experimental evidence is required about possible reaction steps involving OH and H in argon diluted mixtures of CO and O_2 containing controlled amounts of hydrogen.

References

I-1. K. G. P. Sulzmann, B. F. Myers, Jr., E. R. Bartle, General Dynamics/ Astronautics Report GDA-DBE-64-002, February, 1964.

I-2. K. G. P. Sulzmann, J. Quant. Spectry. Rad. Transfer, Vol. 4, 1964, in print.

I-3. A. G. Gaydon, Spectroscopy and Combustion Theory, Chapman and Hall Ltd. London (1948).

I-4. W. E. Kaskan, "The Source of the Continuum in Carbon Monoxide-Hydrogen-Air Flames," Combustion & Flame, 3, 39 (1959).

I-5. A. R. Hochstim, "Equilibrium Compositions, Thermodynamic and Normal Shock Properties of Air with Additives," Vol. I, General Dynamics/ Convair Report ZPh-122, December 1, 1961.

I-6. R. C. Millikan, D. R. White, "Systematics of Vibrational Relaxation," J. Chem. Phys. 39, 3209 (1963).

I-7. J. Daen, P. C. T. DeBoer, "Shock Waves in Argon, Helium, and Carbon Dioxide," J. Chem. Phys. 36, 1222 (1962).

II. INFLUENCE OF H_2 ON THE INDUCTION PERIOD PRECEDING CO_2-FORMATION IN SHOCK HEATED CO-O_2-Ar-MIXTURES - K. G. P. Sulzmann, B. F. Myers, Jr., E. R. Bartle

As has been noted above (Section I), at temperatures around and below 2000°K the apparent activation energy for the induction of CO_2-formation in "dry" mixtures (less than 1 ppm hydrogen containing species) is the same (21 kcal/mole) as measured in a mixture containing 0.1% H_2. It may be expected that below a certain temperature, depending on the amount of H_2 present, for the initiation of rapid CO_2-formation chemical mechanisms become important which are different from those governing the initiation above this temperature. Therefore, studies of the induction period with controlled amounts of H_2 are necessary in order to establish its dependence on the initial concentrations of CO, O_2 and H_2.

During the last two months of the reporting period test data have been obtained for the following mixtures:

10% O_2 + 20% CO + 70% Ar with 0.13% H_2 added,

10% O_2 + 10% CO + 80% Ar with 0.13% H_2 added,

20% O_2 + 10% CO + 70% Ar with 0.13% H_2 added,

20% O_2 + 10% CO + 70% Ar with 0.08% H_2 added.

Analysis of these data as a function of temperature, total gas pressure, and initial concentrations of the reactants is presently being conducted.

At the same time experiments have been performed with a mixture containing 10% O_2, 20% CO and 70% N_2 in order to establish whether the diluent gas has any effect on the reaction mechanisms governing CO_2-formation. The experimental data of these measurements are presently being processed.

III. REVIEW OF LITERATURE ON CO-OXIDATION - B. F. Myers, K. G. P. Sulzmann

The literature search for chemical kinetics data and experimental observations related to the oxidation of carbon monoxide has been extended. During the last month the information obtained has been critically reviewed and a final report[1] has been prepared which will be issued in the near future.

The main result of this review is that at the present time no definite conclusions can be drawn about which are the important reaction steps governing the formation of CO_2. However, technically applicable information about the chemiluminescent radiation in the 2500 - 5500Å region of reacting systems containing CO, O without and with H_2 became available. Under low spectral resolution this radiation appears as a continuous background with a superimposed banded structure.[2] Recent high resolution studies[3] between 4000 and 5800Å indicate that the continuous background consists of a dense rotational fine structure without further underlying true continuum.

Furthermore, the intensity of the chemiluminescent radiation seems to follow the same empirical relationship at total pressures from about 1 mm Hg[4,5] up to 4 atmospheres,[6,7] the total number of quanta emitted per unit volume and time being directly proportional to the concentrations of carbon monoxide and atomic oxygen. This observation is interesting in view of the facts that (a) at the lower pressure limit the emission appears mainly banded without "background" whereas at the upper pressure limit the "background" dominates, and (b) the observed empirical relation is valid also when, e.g. H_2 or C_2H_4 besides N_2 and air is present. From the low pressure data[4,5] and the high pressure observations[6,7] it appears to be reasonable for technical and re-entry applications to adopt the scheme devised by Kaskan[6] for the radiation energy emitted in the total CO-flame band region. This scheme results in the empirical relation

$$I/\text{watts cm}^{-3} = I_o(CO)(O) \quad , \tag{1}$$

where an upper limit for I_o is given by

$$I_o^{max} \approx 2\times10^{12}\, e^{-(3700\pm500)/RT}\ (\text{cm}^3\ \text{mole}^{-1})^2\ \text{watts cm}^{-3} \quad . \tag{2}$$

This expression is based upon the measurements by Clyne and Thrush[4,5]; for a lower limit of the emitted energy, I_o may be expressed by

$$I_o^{min} \approx 7\times10^{11}\, e^{-3200/RT}\ (\text{cm}^3\ \text{mole}^{-1})^2\ \text{watts cm}^{-3} \quad , \tag{3}$$

based upon the measurements by Kaskan.[6]

III-1. General Dynamics/Astronautics Report DBE-64-001.

III-2. A. G. Gaydon, Spectroscopy and Combustion Theory, Chapman & Hall Ltd., London 1948.

III-3. J. H. Callomon, A. C. Gilby, J. Chem. Soc., 1471 (1963).

III-4. M. A. A. Clyne, B. A. Thrush, Proc. Roy. Soc., A269, 404 (1962).

III-5. M. A. A. Clyne, B. A. Thrush, "Ninth Symposium on Combustion," p. 177, Academic Press, 1963.

III-6. W. E. Kaskan, Combustion and Flame, 3, 39, 49 (1959).

III-7. D. R. White, Phys. Fluids, 4, 465 (1961).

IV. COMPUTER CODE FOR CHEMICALLY REACTING, SHOCK HEATED MIXTURE.

K. G. P. Sulzmann, O. R. Hankins

During the last month of the reporting period the IBM-704 chemical kinetics computer program (which we received without cost from Cornell Aeronautical Laboratories, Inc.*) has been adapted for our IBM-7094 computer. The thermo-fit option for the specification of the thermodynamic properties of species as developed at Cornell Aeronautic Laboratories has been included in the code, and all switch options have been replaced by input parameter specifications. The code is presently being recompiled and test calculations will be conducted in the immediate future.

---

* Courtesy of Dr. W. Wurster, Cornell Aeronautical Laboratory, Inc., Buffalo, N. Y.

V. MICROWAVE WAKE INTERACTION STUDIES

A. H. Kritz

In order to aid in the understanding and interpretation of the microwave diagnostic data obtained in probing the wakes of hypervelocity projectiles, all useable microwave data obtained since the start of the measurements program at the NASA Ames Ballistic Range Facility is currently being organized for presentation in a data report. Twenty millimeter hemisphere cylinder projectiles produce the wakes that have been observed employing forward and backscatter C-band and X-band microwaves. The variables in the measurements are model, velocity, range pressure, and range atmosphere (normal, dry air, and dry N_2). The effects of range atmosphere on the electron density in the wake are not apparent in the data reduction because of impurities. Therefore, range atmosphere is not treated as an experimental variable in the data report.

From the forward scattered microwave data, information concerning the magnitude and rate of decay of the linear electron density is obtained. The average linear electron density (Q) and the standard deviation (σ) at one hundred body diameters behind the projectiles are determined from the available data in attempting to define the dependence of the wake structure on the experimental parameters. The decay of electron density (N) in the wake is assumed to satisfy the equation

$$\frac{dN}{dt} = -\alpha N^{\beta+1} \tag{1}$$

so that

$$\frac{1}{N^{\beta}} - \frac{1}{N_o^{\beta}} = \frac{1}{\beta} \exp\left[\frac{\alpha D}{v}\left(\frac{x}{D}\right)\right] \tag{2}$$

where N_o is the initial wake electron density; D is the projectile diameter; v is the projectile velocity; and (x/D) is the distance behind the projectile in body diameters. It is assumed that at 40 body diameters behind the projectile $N^\beta \ll N_o^\beta$ so that the $\frac{1}{N_o^\beta}$ term may be neglected. That Eq. 1 is a reasonable representation of the electron density decay is seen from the fact that the plots of log Q versus log (x/D) are approximately linear. The α's and β's are obtained by fitting a straight line to the data from each shot. The microwave data is obtained in the region of 30 to 800 body diameters with most of the shots yielding data only in the region of 40 to 300 body diameters. In these portions of the wake, it is assumed that the wake cross sectional area, in which the electrons are located, is slowly varying and can be taken as constant in the determination of α and β. This assumption is required because the forward scatter data only yields information about the linear density. The average area for the location of the wake electrons is inferred from the backscatter data. From the microwave data, the dependence of α and β on the experimental parameters is determined.

The average linear electron density, $\bar{Q}$, the standard deviation, σ, $\bar{\alpha}$ and $\bar{\beta}$ derived from the C-band system data are compared with those from the X-band system for shots in which the range pressure, projectile velocity, and projectile model are similar. The projectile velocities are divided into two categories, 17-20 Kft/sec and 20-23 Kft/sec. By similar velocity, it is meant that the velocity is in the same category for the shots considered. In considering similar models all the sodium doped models are taken as the same model. In addition to the dependence of $\bar{Q}$, σ, $\bar{\alpha}$, $\bar{\beta}$ on frequency

employed, the dependence of these quantities on pressure, velocity category, and model are investigated. Data has been obtained at range pressures of 2, 4, 7, 10, 15, 50, and 100 mmHg; in the wake study the models doped with various sodium compounds, teflon capped polyethylene as well as teflon models, and a delrin capped polyethylene model. Any general conclusions which can be inferred from the dependence of the data on the parameters will be included as well as graphs of log Q versus log (x/D). C-band forward scatter microwave data has been obtained from more than eighty shots, and X-band data, from more than fifty-five shots.

A number of analytical radial electron density distributions have been employed in the reduction of the wake backscatter data. For each profile, the effective radius for ionization was determined so that the backscatter data would be consistent with the forward scatter data. C-band reflected microwave data has been obtained from more than forty shots. This data will be presented in the data report and suitable averages will be obtained.

Significant reflected data have not been derived from the X-band microwave system. In an attempt to specify the radial electron distribution some microwave measurements were made at 90° relative to the incident direction. However, inconsistencies from shot to shot have caused these data not to be useful in attempting to characterize the distribution of electrons in the wake. When the X-band microwave horns were moved from 5.5 inches to 16 inches from the wake center, the average linear densities, inferred from the forward scatter data tended to increase. This indicates that the larger portion of the wake illuminated by the incident beam when

the transmitter is removed further from the wake should be taken into account in the data reduction. However, because of variation in parameters such as the water vapor contained in the range atmosphere and the projectile attitude as it travels down the range, the standard deviation of the linear electron density is sufficiently large that the effect of the microwave horn pattern can be neglected.

Because data is now obtained at range pressures higher than those previously employed, it has become necessary to reinvestigate the assumption that the electron-neutral and electron-ion collision frequencies are sufficiently small that they can be neglected in the effective dielectric treatment of the wake. For the C-band and X-band frequencies employed, it is found that in the underdense region of the wake, the effect of collisions on microwave reflection, attenuation, and phase change can be neglected if the ratio of collision frequency to applied angular frequency (ν/ω) is less than or equal to 0.2. For a wake temperature range of 2000 to 4000°K, the maximum range pressure for which this condition would be satisfied is calculated. For example, at 3000°K the wake pressure (and consequently, the range pressure) must be less than 96 mmHg for C-band microwaves; whereas, if a maximum ratio of $\nu/\omega = 0.1$ were allowed at 3000°K the range pressure would have to be less than 58 mmHg. The requirements on the range pressure when the X-band frequency is employed are less stringent.

VI. FLUID DYNAMICS

R. J. Magnus

A. INTRODUCTION

An effort has been made to establish (by use of optical equipment installed at the Ames Range) the radial extent of the turbulent wake at various distances aft of the pellets which are to be fired in the temperature measurement program. A knowledge of the size of the turbulent wake, coupled with an assumption that the ablated sodium is contained within the bounds of the turbulent part of the wake, would facilitate interpretation of the sodium brightness temperature measurements. In addition, certain features of the flow field visible in schlieren or shadowgraph photographs (such as shock shapes, expansion fans, and wake neck size) may be used to augment theoretical conceptions of the "inviscid" flow field about the body.

An account of the use of the optical equipment at Ames to observe firings conducted in January-May 1964 is presented in Section B.

Early in the period it was suspected that the equipment installed at Ames was not sensitive enough to obtain sharply defined photographs of the turbulent wake behind the typical 20 mm diameter blunt pellet (fired at 20,000 ft/sec into air at 50 mmHg pressure) which would be used in the temperature measurement program. It was assumed that alterations would be made to increase sensitivity and, in preparation for this, an estimate was made of the magnitude of the optical disturbances to be sought, (Section C). The gas density disturbances of interest, assumed to be

the density fluctuations at the edge of the turbulent wake (the "turbulent superlayer" of Reference VI-1), are imbedded in the "inviscid" gas density field created by the curved bow shock (and subsequent flow back around the pellet). To see whether or not the turbulent fluctuations might be masked by the "inviscid wake" the deviation of light in the inviscid flow field was estimated, (Section D).

In addition, some engineering data on intensities or "intensity-duration" characteristics of light sources for optical systems was collected, (Section E).

In addition to gathering engineering pre-design information, consideration was given to a suitable optical disturbance for checking sensitivity of optical systems for flow visualization. Section F describes studies of the use of an electrically heated fine wire to set up suitable optical disturbances.

Consideration was given to the use of a heated fine wire as a temperature fluctuation device for probing a turbulent wake. Some very sketchy results are given in Section G.

B. OPTICAL INVESTIGATIONS AT AMES RANGE

The optical system installed at the Ames Range is a conventional Z-type single-pass schlieren apparatus having 10 inch diameter parabolic mirrors with a focal length of 56 inches. The range axis is located midway between the first and second parabolic mirrors (which are about 138 inches apart) and the film plane is about 18 inches beyond the knife edge. A focusing lens can be used to form an image of the test section on the film plane; Polaroid type 47 film is used.

the density fluctuations at the edge of the turbulent wake (the "turbulent superlayer" of Reference VI-1), are imbedded in the "inviscid" gas density field created by the curved bow shock (and subsequent flow back around the pellet). To see whether or not the turbulent fluctuations might be masked by the "inviscid wake" the deviation of light in the inviscid flow field was estimated, (Section D).

In addition, some engineering data on intensities or "intensity-duration" characteristics of light sources for optical systems was collected, (Section E).

In addition to gathering engineering pre-design information, consideration was given to a suitable optical disturbance for checking sensitivity of optical systems for flow visualization. Section F describes studies of the use of an electrically heated fine wire to set up suitable optical disturbances.

Consideration was given to the use of a heated fine wire as a temperature fluctuation device for probing a turbulent wake. Some very sketchy results are given in Section G.

B. OPTICAL INVESTIGATIONS AT AMES RANGE

The optical system installed at the Ames Range is a conventional Z-type single-pass schlieren apparatus having 10 inch diameter parabolic mirrors with a focal length of 56 inches. The range axis is located midway between the first and second parabolic mirrors (which are about 138 inches apart) and the film plane is about 18 inches beyond the knife edge. A focusing lens can be used to form an image of the test section on the film plane; Polaroid type 47 film is used.

Prior to January 1964 the schlieren apparatus was not yielding useable photographs primarily because the luminosity of the flow around the sodium doped models was overexposing the film. This was controlled by restricting the aperture in the vicinity of the knife edge. A blue filter (Corning Glass 556), chosen to surpress sodium radiation, was tried also but the results were indefinite. Photographs of the flow around 20 mm diameter blunt pellets fired at 20,000 ft/sec into air at 50 mmHg pressure were made during January 1964, using a spark source with a nominal duration of 0.4 microseconds. The shapes of the bow and trailing shocks, outlines of the separated flow at the pellet base and density gradients in the "inviscid wake" were clearly visible but there was no evidence of either a laminar or turbulent viscous wake; the flow was expected to be turbulent.

It was subsequently determined that the spark source used in the January attempts contained faulty energy storage capacitors. The unit was repaired and, when tests resumed in April, the photographs made using a nominal light source duration of 0.1 microseconds were definitely sharper than those made during January. There still was insufficient sensitivity in the system to show clearly the turbulent wake.

A shadowgraph made with the camera focused on a plane 3 feet closer than the plane containing the range axis showed flow details comparable to those obtained with the schlieren system.

Efforts are being made to improve the sensitivity of the optical system but without extensive modifications. Alternatively, attempts to obtain information as to the distribution of sodium in the wake will be made using an image converter camera with filter to photograph directly the sodium emission.

C. OPTICAL DISTURBANCE DUE TO A TURBULENT WAKE EDGE

Assume that the edge of the turbulent wake behind a hypervelocity pellet is composed of segments of spherical surfaces of various radii. To estimate the deviations of light penetrating the wake in the vicinity of the turbulent edge it will be assumed that the spherical segments contain air which is hotter (and less dense) than the air in which the wake is immersed. Since the optical effects are expected to be greatest in the vicinity of the edge of the bubble of hot gas, the model for calculating the effects at the edge of the bubbles can be taken as an isolated single spherical bubble. In the work which follows this model has been considered from two viewpoints. First, the edge of the bubble was considered to be a sharply defined discontinuity and geometric optics was used to estimate the light ray deviations which could be expected (directly useable for calculating responses of schlieren systems) and the illumination intensity patterns which could be expected on planes representing the film planes of shadowgraph systems. Second, the bubble was considered to be bounded by a linear density gradient region of small thickness (a turbulent superlayer) and the central portion of the bubble was assumed to have a uniform density. This model was considered from the point of view of physical optics and the phase shifts of wave fronts traversing representative bubbles of this type were calculated.

Deflection of a Light Ray

Consider, therefore, a spherical bubble of radius R, containing material of index of refraction n_2 immersed in a medium of index of refraction n_1; see Figure VI-1. A light ray coming from the positive Z direction and intersecting the bubble at $y = R \cos \theta$ will be deflected upon traversing the bubble by an angle ϵ. If n_1 is greater than n_2 and both are very nearly equal to one, then according to Snell's law:

$$\epsilon \doteq 2\left(\frac{n_1}{n_2} - 1\right) \cot \theta = 2\left(\frac{n_1}{n_2} - 1\right) \frac{\left(\frac{Y}{R}\right)}{\sqrt{1 - \left(\frac{Y}{R}\right)^2}} \qquad (1)$$

This approximation is applicable provided that total reflection does not occur; it is valid then if:

$$\frac{n_1}{n_2} \cos \theta < 1$$

For this analysis it is permissible to neglect the totally reflected part of the light.

Schlieren System Performance

In this model, the angular deflection of the light ray is independent of bubble size and depends only on the indexes of refractions and the angle at which the ray strikes the bubble. The deflection of the ray is a quantity of direct interest for the calculation of the expected response of a schlieren optical system. For a conventional single pass Z-type system the ray deflection ϵ will cause a fractional change of illumination at the film plane of:

$$\frac{\Delta I}{I_o} = \frac{\epsilon f}{h} \qquad (2)$$

where f is the focal length of the second parabolic mirror and h is the height (normal to the knife edge which is assumed to be parallel to the Y axis) of that part of the image of the light source (assumed to be a rectangle with 2 sides parallel to the knife edge) which is permitted to pass the knife edge when no disturbance is present. This expression (2)

assumes that the light source is uniform in intensity and that ef is small enough that the light is neither completely cut off nor all allowed to pass; see Reference VI-2 or any text on schlieren systems. Ordinarily a relative change in illumination of 0.10 is considered detectable but when extremely weak phenomena are to be observed (as they are in the situation of interest here) other considerations than relative change of illumination intensity may determine the visibility.

According to Eq. (1) the value of ϵ would be zero for a ray penetrating the bubble at $\frac{y}{R} = 0$ and would tend toward a maximum as the point of penetration was raised toward $\frac{y}{R} = \frac{n_2}{n_1}$, (the totally reflected rays are being ignored). For very small differences in the indexes of refraction of the two media it may occur that the change of illumination in the image of the bubble on the film plane is negligible except in a very narrow zone near the outside of the bubble. Then the visibility of this very narrow line might need to be determined by comparison of the line width with the resolutions of the optical system or the film.

From this qualitative discussion it would be expected that the schlieren photographs of the turbulent trails of pellets fired into very rarefied air would appear very "flat"; that is, only the portions of the turbulent boundary viewed at nearly grazing incidence would differ appreciably in illumination from the undisturbed field. The photograph shown on p. III-11 of Reference VI-3 has this appearance.

For typical experimental conditions the Ames Range (a 20 mm pellet fired into 50 mmHg air at 20,000 ft/sec) it was estimated that the temperature of the "inviscid wake" might be 1600°K and that the tempera-

ture of the edge of the turbulent wake might be 2000°K at 20 diameters aft of the pellet. These values imply that $n_1 = 1 + 3.28 \times 10^{-6}$ and $n_2 = 1 + 2.63 \times 10^{-6}$. It was, further guessed that the radii of curvature of the turbulent wake surface "pebbles" might be anywhere from 3×10^{-2} to 3 cm. The values of ϵ for bubbles having the indexes of refraction mentioned are shown in Figure VI-2.

For the schlieren system in use at the Ames Range f = 142 cm and h of 0.01 cm seems reasonable. Then, from Eq. (2) an ϵ of 7×10^{-6} radians should cause a 10% change in illumination. From Figure VI-2, therefore, a 10% darkening could be expected only over the outer 5% of the bubble radius. For a bubble of radius of 3 cm the bubble edge line width expected on the film (where the image linear size is about 1/3 the object size) was 5×10^{-2} cm; this was expected to be visible. On the other hand the line (at the film plate) created by a bubble of 3×10^{-2} cm radius was expected to be only 5×10^{-4} cm wide and probably not visible because of limited film resolution.

Shadowgraph Effects

Referring again to Figure VI-1, if uniform parallel light is incident upon the bubble-like disturbance of index of refraction in the medium, it will be turned through an angle ϵ depending on the radius y (y now is being regarded as a radial coordinate in a cylindrical system whose axis is Z) at which the particular ray encounters the bubble. If the light then is allowed to fall on another plane normal to Z but displaced a distance L ($L \gg R$) from the point at which the disturbance is centered, the illumination will not be uniform because the rays will have been spread

apart in some regions and piled up in others, see Figure VI-1. A shadowgraph may be obtained by exposing a film at some plane which is a distance L from the disturbance.

Quantitatively, the shadowgraph effect may be estimated by observing that a ray penetrating the disturbance bubble at a distance $\frac{y}{R}$ from the Z axis will strike the film plane at a distance $\frac{\eta}{R}$ from the Z axis, (Figure VI-1), where:

$$\frac{\eta}{R} = \frac{y}{R} + \epsilon \frac{L}{R} \tag{3}$$

To calculate the illumination in the η plane due to rays which have crossed the disturbance [$I(\eta)$ will be regarded as the number of rays per unit area of the η plane] we may observe that, since η is a monotonic increasing function of y, that all rays which cross the y plane in a circle of radius y cross the η plane within a circle of radius η:

$$2\pi \int_0^{\eta} I(\eta)\, \eta d\eta = 2\pi \int_0^{y} I_o\, y dy = \pi I_o y^2$$

where I_o is the uniform illumination incident upon the disturbance. Upon differentiating the integrals it will be found that:

$$\frac{I(\eta)}{I_o} = \frac{y}{\eta} \frac{1}{\left(\frac{d\eta}{dy}\right)} \tag{4}$$

The value given by Eq. (4) is less than one (for $n_2 < n_1$) and indicates that the central portion of the shadow of the disturbance is darker than the undisturbed field. Outside the circle of radius $\frac{\eta}{R} = 1$, however, the light which passed outboard of the bubble also falls on the η plane and the illumination is:

$$\frac{I(\eta)}{I_o} = 1 + \frac{y}{\eta} \frac{1}{\left(\frac{d\eta}{dy}\right)} \qquad (5)$$

The illumination distributions on the film plane depend not only on the indexes of refraction but also upon the distance of film from the disturbance, $\frac{L}{R}$. For the same conditions as mentioned above in discussing schlieren performance the illumination distributions on film planes at $\frac{L}{R}$ of 25 and 6000 (thought to represent extremes of some sort; $\frac{L}{R} = 25$ for L = 75 cm and R = 3 cm, and $\frac{L}{R} = 6000$ for L = 180 cm and R = 0.03 cm) are presented in Figures VI-3 and VI-4. Note that the widths of the lines over which the illumination is changed by 10 percent from the background illumination are quite small, amounting to only 0.011 cm total width for the dark and bright line pair shown in Figure VI-3 and only 0.005 cm for the pair in Figure VI-4.

Whether or not these lines might be visible depends upon the angular dispersion in the "parallel" beam due to finite dimensions of the light source. For the optical system in use at Ames the beam dispersion might be $\delta = 9 \times 10^{-5}$ radians (for a circular source 0.005 inches in diameter 56" from a parabolic mirror used to create a "parallel" beam). The shadow patterns on the film resulting from parallel light are shown in Figures VI-3 and VI-4; because of non-parallelism, the patterns resulting from individual points of the light source must be superimposed in an array which is spread over the film plane by an amount $L\delta$ or 7×10^{-3} cm for the case represented in Figure VI-3 and 1.6×10^{-2} cm for the case represented in Figure VI-4. If the spread due to finite source size is large compared to the width of the line pair due to point source the

disturbance would not be visible because of cancelling of bright and dark lines. On this basis, the shadowgraph of Figures VI-3 is considered marginally visible but there is very little hope that the shadowgraph of Figure VI-4 would be visible.

The foregoing analysis is highly idealized and care should be taken not to extend it unduly. With this in mind the order of magnitude of the thickness of the turbulent superlayer of the wake mentioned was estimated (on the basis of information in Reference VI-1) to be 1.2×10^{-2} cm. If it is assumed that the index of refraction of the spherical bubble varies linearly from n_1 to n_2 as the radial distance from the center is decreased by 1.2×10^{-2} cm from the maximum radius R, then a more complicated integration must be used to calculate ϵ vs y/R and the result will depend on R. The values of ϵ vs y/R for $R = 3 \times 10^{-2}$ cm and 3 cm (assuming a 1.2×10^{-2} cm thick superlayer) are shown as dotted curves in Figure VI-2. Without going into detail, the result for the deflection of a ray crossing a bubble where the index of refraction varies linearly from n_2 at radius R_2 to n_1 at outer radius R_1 is:

$$\epsilon = \frac{2\left(\frac{n_1}{n_2} - 1\right)}{1 - \frac{R_2}{R_1}} \frac{y}{R_1} \log \frac{1 + \sqrt{1 - \left(\frac{y}{R_1}\right)^2}}{\frac{R_2}{R_1} + \sqrt{\left(\frac{R_2}{R_1}\right)^2 - \left(\frac{y}{R_1}\right)^2}}$$

for $y < R_2$

and

$$\epsilon = \frac{2\left(\frac{n_1}{n_2} - 1\right)}{1 - \frac{R_2}{R_1}} \frac{y}{R_1} \log \frac{1 + \sqrt{1 - \left(\frac{y}{R_1}\right)^2}}{\left(\frac{y}{R_1}\right)}$$

for $R_2 < y < R_1$.

The principal result of including a finite skin depth in the model for the bubble is that the possibility of the 0.03 cm bubble being visible with the present optical system is made more remote. No estimates of shadowgraph performance were made using the more complicated bubble model.

Physical Optics Description of Bubble Model

Since the disturbances which one would like to picture using an optical system are quite small, it is possible that limitations of a physical type might occur; that is, geometric optics might be insufficient for an accurate analysis. It was planned to analyze the performance of the schlieren system by physical optics in a manner similar to that given in Reference VI-4; however, this work has been suspended. Only the descriptions of the disturbances sought have been completed.

Spherical bubbles with a constant index of refraction in the interior, bounded by a skin (in which the index of refraction varies linearly with radius), suspended in a uniform medium of greater index of refraction were taken as a model.

The disturbances in optical pathlength in traversing the bubbles were calculated as functions of $\frac{y}{R_1}$ for 3 bubbles having the following properties:

Index of Refraction of External Medium	$1 + 3.28 \times 10^{-6}$
Index of Refraction of Bubble Material	$1 + 2.63 \times 10^{-6}$
Outer Radius of Bubble	3×10^{-2} cm 3×10^{-1} cm 3 cm
Skin Thickness of Bubble	1.2×10^{-2} cm

The results are presented in Figure VI-5. The disturbance to optical pathlength amounts to only 0.1 wave length through the center of the

3 cm bubble (a wave length of 4×10^{-5} cm was assumed).

D. DEVIATION OF LIGHT IN INVISCID WAKE

Inasmuch as the density gradients in the inviscid wake were clearly visible in schlieren photographs taken in January but the turbulent wake was not visible, an estimate was made of the optical disturbances which could be expected in traversing the inviscid wake.

The estimation was carried out for a plane 20 diameters aft of a 20 mm blunt pellet fired at 20,000 ft/sec into air at 50 mmHg pressure. The inviscid flow field was approximated (roughly following blast wave theory) by assuming similar density profiles behind a locally conical bow shock. The bow shock radius was considered to be given by:

$$r_s = 7.70 + 0.10\ (x-40) \text{ centimeters}$$

where x is the distance aft of the pellet in centimeters. The similar density profiles were assumed to have zero density out to 0.9 of the shock radius and to vary parabolically up to the shock.

$$\rho = 0 \qquad r \leq 0.9\ r_s$$

$$\rho = 100\ \rho_s \left(\frac{r}{r_s} - 0.9\right)^2 \qquad 0.9\ r_s < r \leq r_s$$

The density at the shock was assumed to vary with distance aft of the pellet

$$\rho_s = 0.159 - 3.16 \times 10^{-4}\ (x-40) \text{ amagat.}$$

The entire flow field was considered to be imbedded in air of density 6×10^{-2} amagat.

The deviations of rays of light proceeding in the -Z direction (see Figure VI-6) were calculated by using Snell's law for the deviations

in penetrating the shock (inward and outward) and simple integrations (involving the density gradients) through the shock layer:

$$\epsilon_x = \epsilon_{x\ \text{shocks}} + \int_{\text{shock layer}} k \frac{\partial \rho}{\partial x}\, dz$$

where k is the Gladstone-Dale constant for air. An analogous expression was used for obtaining the ray deviation in the y direction.

The results, the deviations in radians expected are given in the table below:

Height of Entering Ray (y/R)	Deviation in + x-direction	Deviation in + y direction
0	4.65×10^{-6}	0
0.5	-1.73×10^{-5}	2.28×10^{-5}
0.87	-3.85×10^{-5}	9.4×10^{-5}
0.98	-2.67×10^{-5}	3.2×10^{-5}

Comparison of these ray deviations with those expected as a result of penetrating the edge of the turbulent wake suggests that:

(a) The density gradients of the inviscid wake are probably more readily made visible by a schlieren system than the turbulence.

(b) It may be necessary to take account of the darkening or lightening of the picture due to the effect of the inviscid wake in order to obtain the best exposure for seeing the turbulence.

E. SURFACE BRILLIANCE OF LIGHT SOURCES

For calculating the performance of optical systems designed to

observe fast moving objects, the intensity-time characteristics of the light sources must be known since the film must be exposed before the image has been blurred by object motion. Empirical data on the time-integrated light output of 4 spark sources has been gathered using the exposure of Type 47 Polaroid film as an indicating device. In addition, since the flow about the pellets used in the Ames experiment is self-luminous due to the added sodium, there is a possibility of over-exposing the film; the integrated intensity of the self-luminosity was also evaluated.

It was assumed that Polaroid Type 47 film is correctly exposed by 7.8×10^{-5} meter candle seconds, a number deduced from data given on pages 64 and 67 of Reference VI-2 (meter candle = $\frac{\text{candle}}{\text{stere meter}^2}$); the geometric optics and losses at various optical elements in the optical system installed at Ames were accounted for and a number was deduced for the light output. Two different energy storage units may be used and values were deduced for both units; in the sources used at Ames the spark occurs in air at atmospheric pressure. The wake luminosity was deduced in a similar manner. Two other types of sources were investigated both based upon elements of the AVCO LS-020 packaged light source. In one, used essentially as-is, the spark takes place in air but is confined by ceramic baffles so that a high pressure may develop. This unit was also tested in a modified version; the spark was made to take place in a low velocity argon jet flowing from one of the electrodes. Because the break-down voltage of argon is low the energy storage of the source when used in this form is quite low. The evaluations of the high-pressure source and argon arc source were made in a large dark room; that is no corrections

for optical elements were introduced.

The results are listed in the table below:

	Nominal Duration (microseconds)	Energy Input (watt seconds)	Time-Integrated Surface Brilliance, ($\frac{\text{candle seconds}}{\text{cm}^2 \text{ stere}}$)
Unconfined spark in air	0.4	36	0.3
Unconfined spark in air	0.1	12	0.16
Confined spark in air	1.2	10	1.9
Arc in argon column	1.2	2.5	0.2
Wake of 20 mm polyethylene + 10% sodium acetate pellet fired at 20,000 ft/sec into air at 50 mmHg	-	-	1.3×10^{-3}

F. USE OF HEATED WIRE AS OPTICAL TEST OBJECT

The use of a heated fine wire to set up optical disturbances for checking sensitivity of optical systems was investigated. Use of a wire for this purpose has several advantages; first, the disturbances set up have a character much like those which will be observed when the system is used for flow visualization; second, the magnitude of the optical disturbance can be varied greatly by controlling the electrical current in the wire (which determines wire temperature) or the pressure of air in the test cell or the aspect by which the wire is viewed; and third, the test object is relatively small and could be used for last-minute checking of systems at a ballistic range.

A hot-wire test object was constructed by soldering a 1 cm length of 0.0013 cm diameter tungsten wire between two needle-like supports. A

heating current of up to 125 milliamperes could be supplied to the wire which had a resistance of about 7 ohms at room temperature. This current is sufficient to heat the wire about 300°C at atmospheric pressure. The wire was mounted in a cylindrical cell about 8 cm in diameter which was equipped with windows in the ends and could be evacuated. The mount of the wire in the cell was arranged so that the wire could be rotated and viewed normally or "end on".

Tests were carried out at atmospheric pressure using a simple shadowgraph system. The wire was viewed along its' axis and photographs were taken with several wire heating currents and varying distance from test object to film plane. The evaluations were made by using a "handbook" value for the temperature coefficient of resistivity of the wire and the measured wire resistance to get the wire temperature. It was then assumed that the heat would be conducted away from the wire by the air; this provided an estimate of the density field. Calculations for the diameter of the shadow which could be expected were carried out by a method similar to that described in Section C. The diameter of the shadowgraph cast by the wire estimated by this rough procedure was about 60% of the value measured.

G. FEASIBILITY OF USING HOT WIRE FOR PROBING WAKE

It has been suggested that a hot wire anemometer might be used for probing the turbulent wakes behind hypervelocity projectiles. To investigate the feasibility of this suggestion some comparisons were made of the dynamic pressures which could be expected in wind tunnel and ballistic range work and then a hot wire was installed in the ballistic range at Ames for survival

heating current of up to 125 milliamperes could be supplied to the wire which had a resistance of about 7 ohms at room temperature. This current is sufficient to heat the wire about 300°C at atmospheric pressure. The wire was mounted in a cylindrical cell about 8 cm in diameter which was equipped with windows in the ends and could be evacuated. The mount of the wire in the cell was arranged so that the wire could be rotated and viewed normally or "end on".

Tests were carried out at atmospheric pressure using a simple shadowgraph system. The wire was viewed along its' axis and photographs were taken with several wire heating currents and varying distance from test object to film plane. The evaluations were made by using a "handbook" value for the temperature coefficient of resistivity of the wire and the measured wire resistance to get the wire temperature. It was then assumed that the heat would be conducted away from the wire by the air; this provided an estimate of the density field. Calculations for the diameter of the shadow which could be expected were carried out by a method similar to that described in Section C. The diameter of the shadowgraph cast by the wire estimated by this rough procedure was about 60% of the value measured.

G. FEASIBILITY OF USING HOT WIRE FOR PROBING WAKE

It has been suggested that a hot wire anemometer might be used for probing the turbulent wakes behind hypervelocity projectiles. To investigate the feasibility of this suggestion some comparisons were made of the dynamic pressures which could be expected in wind tunnel and ballistic range work and then a hot wire was installed in the ballistic range at Ames for survival

tests.

It was assumed that the hot wire probe must be mounted somewhere between say 1.5 and 3 pellet radii off axis in order that the turbulent wake would grow outward and engulf the probe within the time that the pellet had traveled say 100 diameters past the probe location. Rough calculations were then carried out of the dynamic pressure to which the hot wire would be suddenly subjected as the result of passage of the bow shock from a blunt projectile traveling at 20,000 ft/sec in air at 50 mmHg. The dynamic pressures were respectively 30 atmospheres and 2.2 atmospheres at 1.5 and 3.0 radii off axis. For comparison, in the wind tunnel tests reported in Reference VI-5, wires were frequently broken during tunnel starting; it is estimated here that the wind tunnel dynamic pressure was about 0.14 atmosphere.

A probe using a 1 cm length of 0.0013 diameter tungsten wire was installed in the Ames Range for monitoring some firings of 1/2" diameter aluminum spheres at 12,000 ft/sec into air at 4 mmHg pressure. Three tests were monitored; on the first two shots the wire was 12 radii off axis and on the third shot, 8 radii off axis. The wire did not survive the firing and subsequent events on the first and third shots. On the second shot the wire survived and oscillograph traces of the voltage drop across the wire were obtained; they showed no detectable signal although sensitivity sufficient to detect a 10°C change in wire temperature had been used.

The results, while inconclusive, were not sufficiently encouraging to warrant further effort.

REFERENCES

VI-1. Corrsin, Stanley and Kistler, Alan L., "The Free-Stream Boundaries of Turbulent Flows," NACA TN 3133, January, 1954.

VI-2. Holder, D. W. and North, R. J., Schlieren Methods, National Physical Laboratory, Notes on Applied Science No. 31, Her Majesty's Stationery Office, London, 1963.

VI-3. Reentry Physics and Project Press Programs, Semiannual Technical Summary Report to the Advanced Research Projects Agency, Massachusetts Institute of Technology, Lincoln Laboratory, 9 February 1962.

VI-4 Shafer, H. Jerome, "Physical Optic Analysis of Image Quality in Schlieren Photography," Journal of the SMPE, Vol. 53, p. 524-544, November 1949.

VI-5. Dewey, C. Forbes, Jr., "Hot Wire Measurements in Low Reynolds Number Hypersonic Flows," A.R.S. Journal, Vol. 31, No. 12, p. 1709, December, 1961.

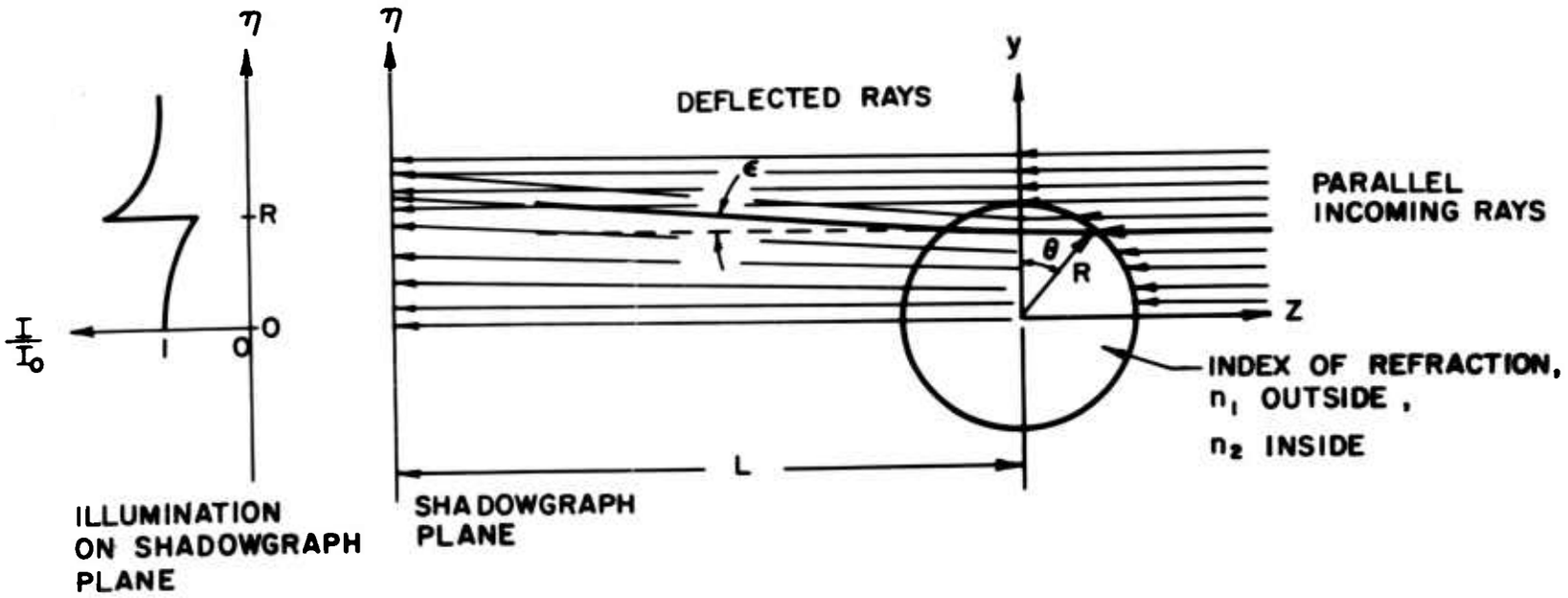

FIGURE VI - 1 : SIMPLE SPHERICAL BUBBLE MODEL FOR ESTIMATING SCHLIEREN AND SHADOWGRAPH EFFECTS.

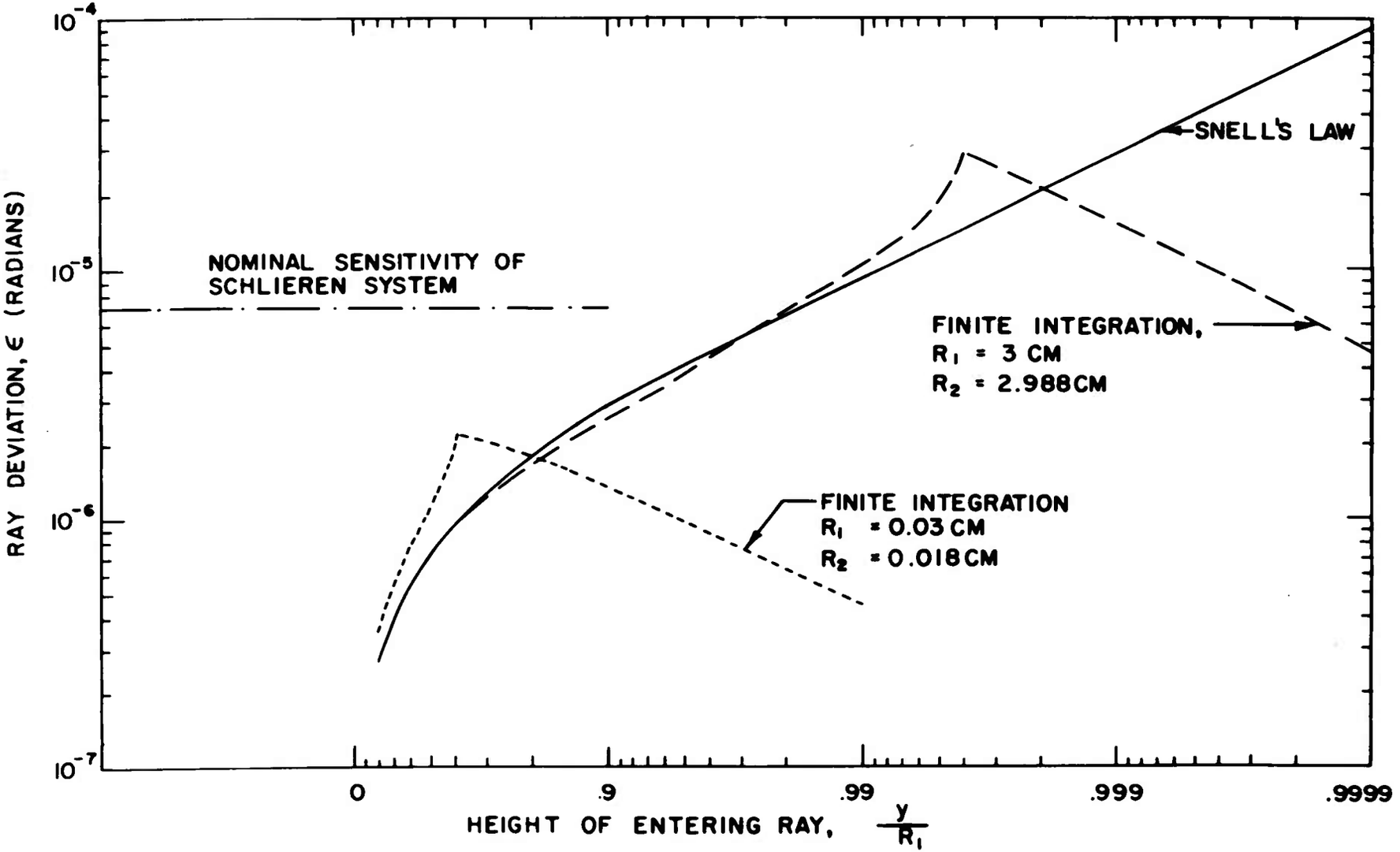

FIGURE VI-2 : DEVIATIONS OF LIGHT RAYS IN CROSSING SPHERICAL DISTURBANCES OF INDEX OF REFRACTION.

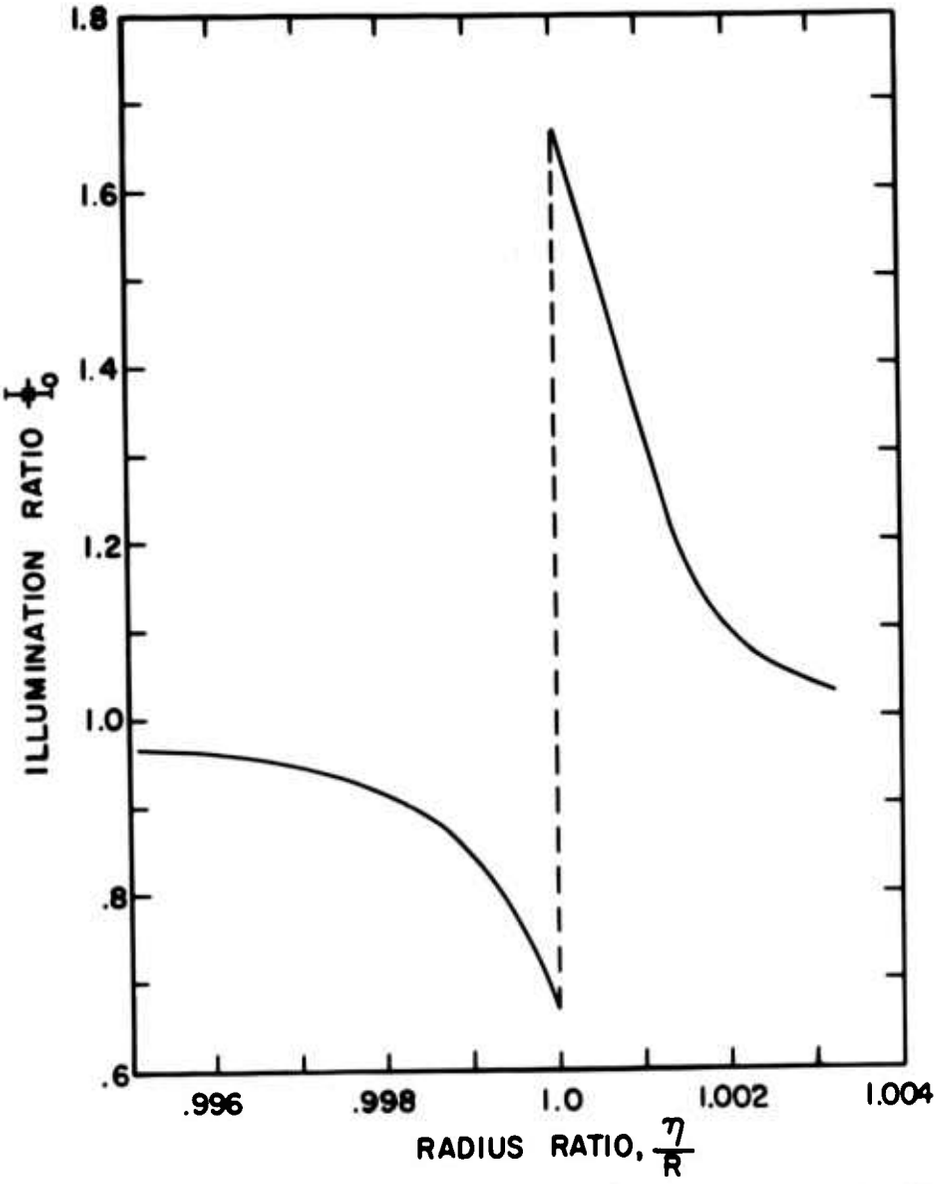

FIGURE VI - 3 : SHADOWGRAPH OF SPHERICAL DISTURBANCE IN INDEX OF REFRACTION ON A PLANE 25 RADII FROM THE DISTURBANCE.

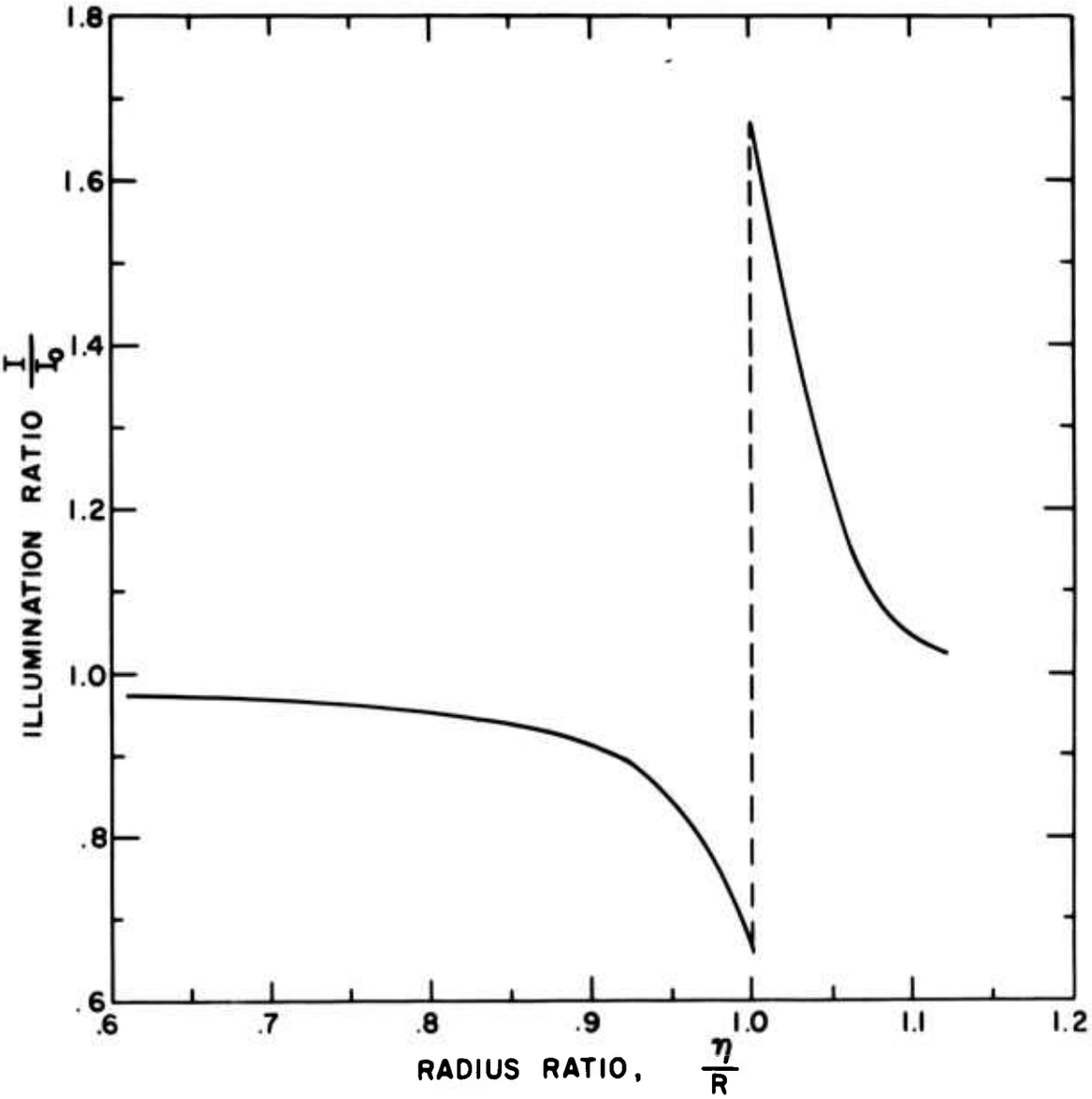

FIGURE VI - 4 : SHADOWGRAPH OF SPHERICAL DISTURBANCE IN INDEX OF REFRACTION ON A PLANE 6000 RADII FROM THE DISTURBANCE.

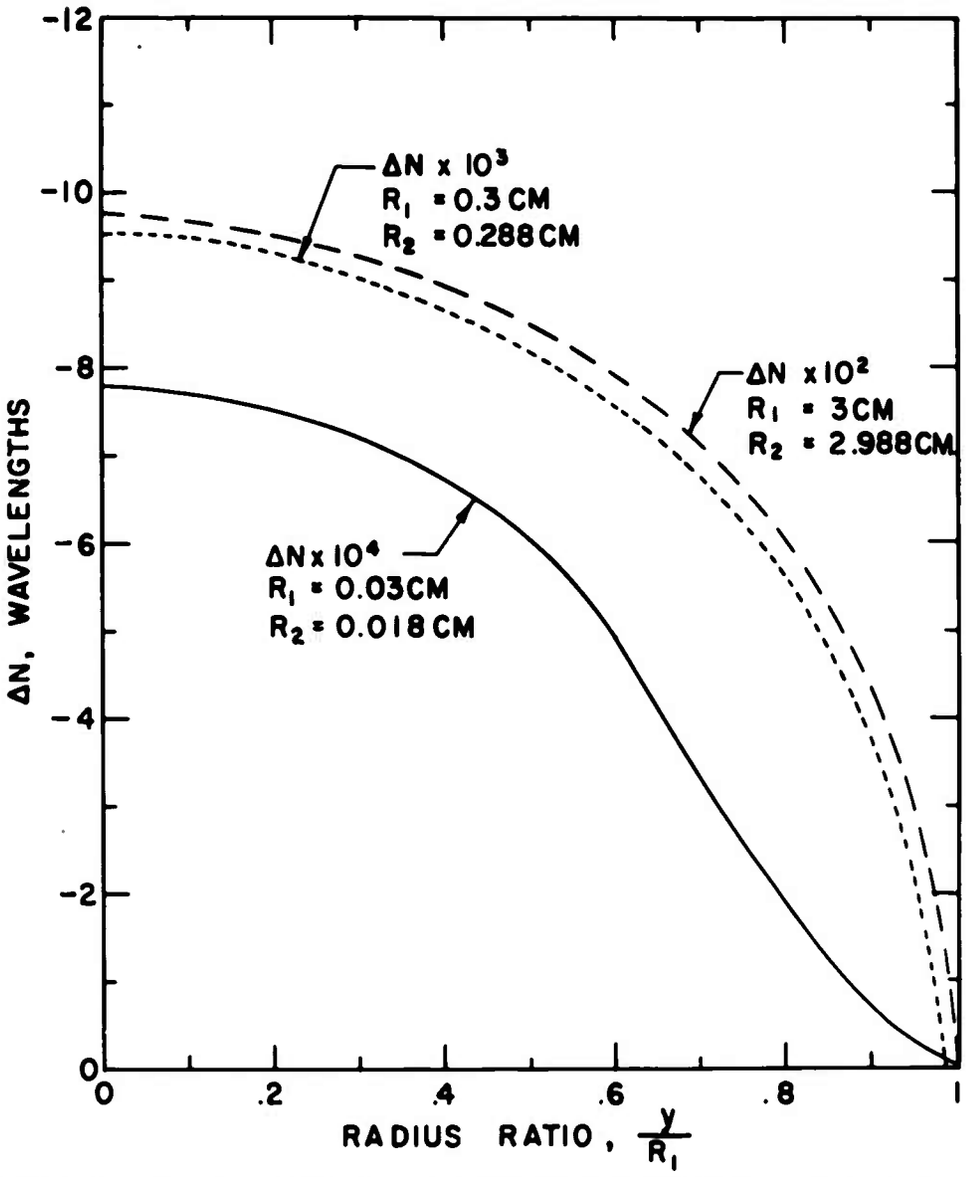

FIGURE VI - 5 : OPTICAL PATH DISTURBANCE DUE TO CROSSING A SPHERICAL DISTURBANCE IN INDEX OF REFRACTION.

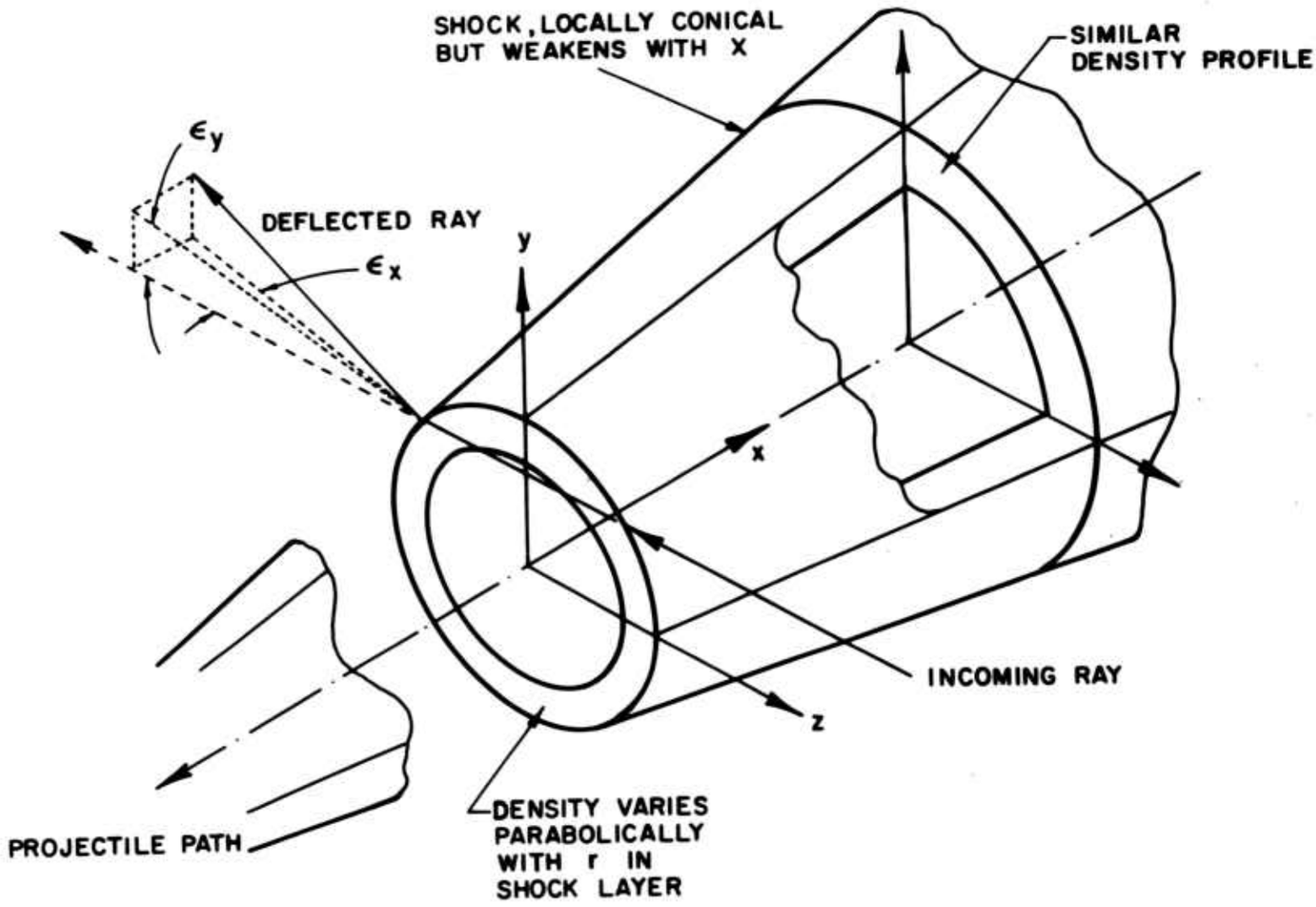

FIGURE VI - 6 : MODEL USED FOR ESTIMATING RAY DEVIATIONS IN THE INVISCID WAKE.

VII. HYPERVELOCITY WAKE TEMPERATURE MEASUREMENTS - W. J. Hooker and P. R. Erickson

During this first half of the contract period, the apparatus for making repetitive wake temperature measurements,[1] utilizing a spectral line reversal technique, was completed and is shown schematically in Fig. VII-1. Light from the source is imaged in the center of the Kerr cell. Both polarizers are set at an angle of 45° to the electric vector of the Kerr cell, and are parallel to the slit of the monochromator for maximum signal. (Since the grating used for dispersion has a ruling of 1800 lines/mm, the line spacing is comparable to the wavelength used and, hence, has a polarizing effect.) The light source is subsequently imaged onto the axis of the test section and then onto the entrance slit of the monochromator. All of the optics used are overcoated with magnesium fluoride to reduce reflection losses.

After dispersion within the monochromator, two adjacent wavelength intervals are selected with the beam-splitter arrangement shown in Fig. VII-1(b). With a basic reciprocal dispersion of 18Å/mm, this results in a resolution of better than 1Å in each channel, with a 10Å separation in the first order.

The light source, Kerr Cell Filter and lenses on one side of the gun range are mounted on a one-piece channel optical bench, which can be accurately moved in the vertical plane with respect to a support framework which is rigidly attached to the test section. The monochromator, lens and photomultipliers are mounted in a similar manner on the opposite side of the test section. Off-axis traverses are obtained by placing machined spacers under each optical bench, thereby offsetting them from the original boreline.

The overall sensitivity of each channel is controlled by varying the load resistance in the anode circuit of the photomultipliers used to detect the light signals. The photomultiplier circuit employed is shown in Fig. VII-2.

The feeder current was chosen so that the photomultipliers would have identical AC and DC gain, and the load resistances were selected so that the frequency response was flat from DC to 35 kc, using a mechanical square-wave light chopper.

The apparent brightness of the light source is changed by application of a voltage to the Kerr cell plates, which alters the transmission[2,3] of the Kerr Cell Filter. In Fig. VII-3 is shown the measured transmission of the system employed, as compared with calculations, for DC voltage. In this measurement, the polarizers were crossed at 90° with respect to each other.

As the Kerr Cell Filter transmission changes from minimum to maximum, the apparent source temperature varies in an analogous manner. Therefore, by applying a cyclically varying voltage waveform to the Kerr cell plates, we produce an effective source temperature variation of the same frequency. The circuit chosen for this function is shown in Fig. VII-4.[4] The principle of this circuit is to maintain one of the Kerr cell plates at the potential of the high voltage power supply, 35,000 volts DC, while the potential of the other plate is varied by the desired voltage waveform between 35,000 volts DC and 1000 volts DC. The waveform, either sine wave or sawtooth voltage, is produced by the Function Generator. The repetition rate of this voltage waveform may be selected at any frequency between 10,000 and 100,000 cycles per second. When a trigger pulse is delivered to the External Trigger input, both the waveform from the Function Generator and the pulse voltage, one millisecond duration, from the Pulse Generator are delivered to the Mixer-Amplifier. In this unit, the waveform is added to the pulse as shown in Figure VII-4. This signal voltage is then supplied to the Linear Amplifier with a gain of about 100, where the signal is increased to about 300 volts peak amplitude. The Linear Amplifier supplies the signal voltage to modulate

the control grid of the Tetrode. This signal voltage is adjusted so that the Tetrode operates over the linear portion of its plate characteristics curve. When no signal voltage is present at the grid, the Tetrode is cut off. The modulation of the control grid causes the Tetrode to conduct, thus dropping the potential of its plate circuit and developing the net change of plate potential across the Resistor Bank. Since the Kerr cell is electrically parallel to the Resistor Bank, the change in plate potential also appears across the Kerr cell. Thus, the Kerr cell is modulated by the waveform which appears as a change of potential between its plates. The modulation voltage can be adjusted to 34,000 volts DC at a repetition rate between 10,000 and 100,000 cycles per second for a one millisecond duration as shown in the photograph in Figure VII-4. This photograph also indicates that the Kerr Cell is only 80% modulated with the waveform; 20% of the potential across the Kerr cell is pulse voltage which allows more efficient use of the modulation voltage by biasing the Kerr cell above the flat portion of the Kerr cell transmission characteristics curve (see Fig. VII-3)

In Fig. VII-5 are shown two oscilloscope traces of the outputs of the photomultipliers monitoring radiation at λ_1 (5890Å) and λ_2(5880Å). The top trace shows the identical response of the two channels to the Kerr cell-modulated source radiation. The Kerr cell is being modulated at a basic 20 kc linear sawtooth frequency, and the polarizers are parallel to each other. Note the transient initial cycle when the modulator is gated on. The bottom trace shows the resultant signal when both channels are fed into a differential preamplifier prior to recording. In this trace, we see that virtually all signs of the modulation have been removed, indicating an almost complete null over the entire cycle. This, then, will allow us to measure wake line reversal temperatures by noting the source brightness temperature at the time a null occurs in the modulation cycle.

References

VII-1. Space Science Laboratory, "Re-Entry Physics Research Annual Report," General Dynamics/Astronautics, Report No. GDA-DBE-64-010, March 1964.

VII-2. Kingsbury, E. F., Rev. Sci. Instr. 1, 22 (1930).

VII-3. Zarem, A. M., Marshall, F. R., and Poole, F. L., Elec. Eng. 68, 242 (1949).

VII-4. Designed and developed by Waddell Dynamics, Inc., San Diego, California.

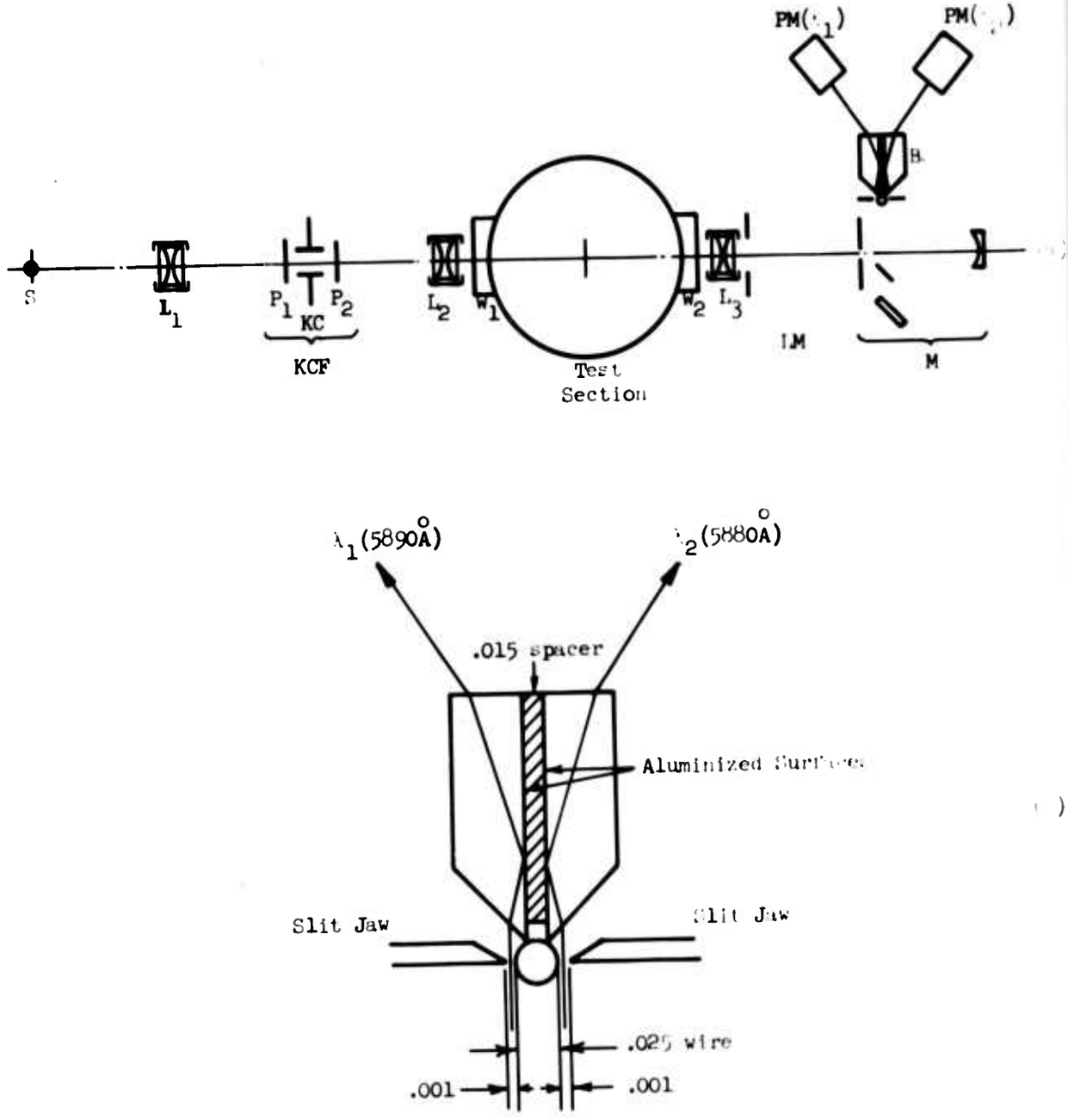

Fig. VII-1. Optical System Used for Temperature Measurements

RCA 7265 Photomultiplier Tube

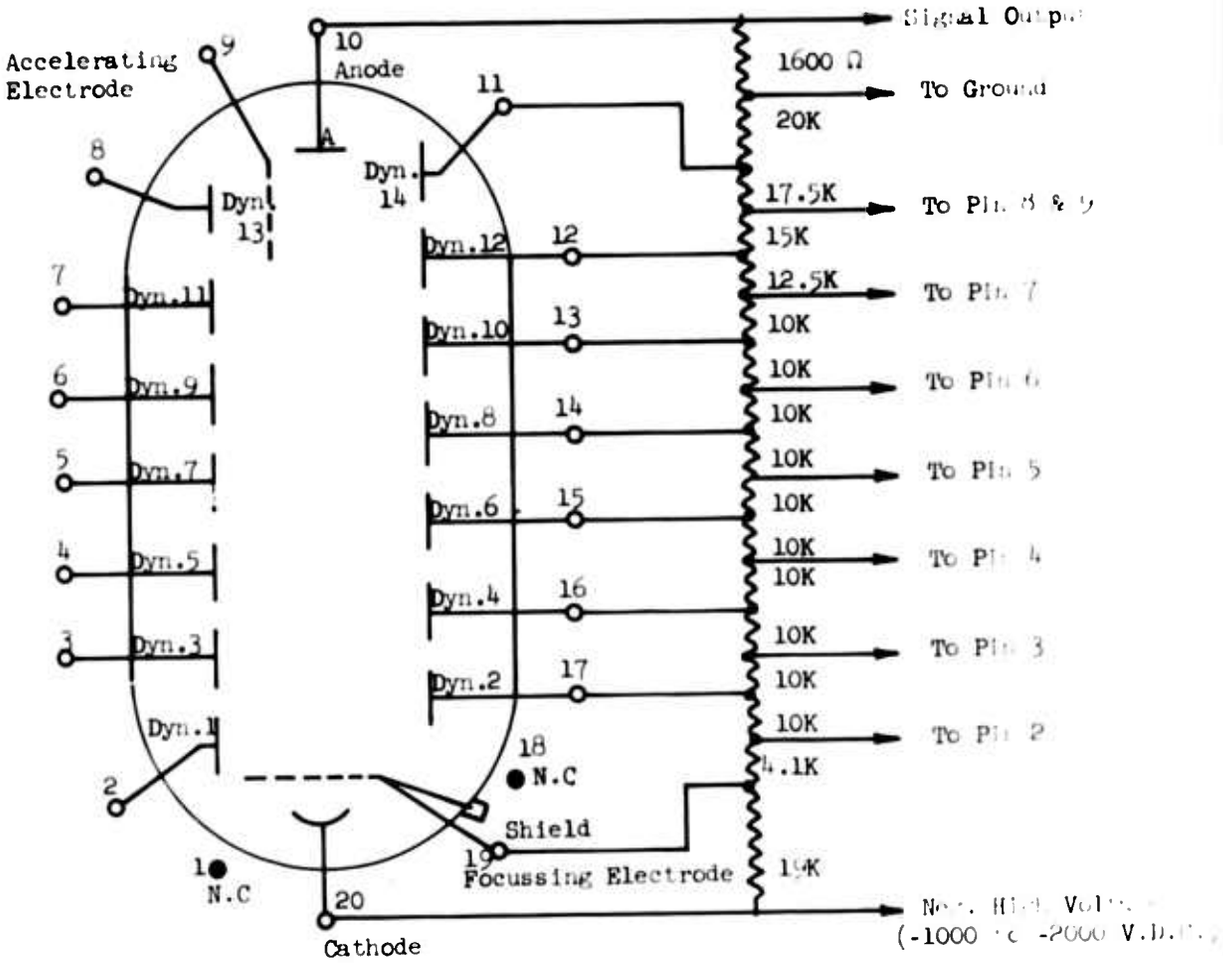

Fig. VII-2. Photomultiplier Tube Amplifier - Schematic

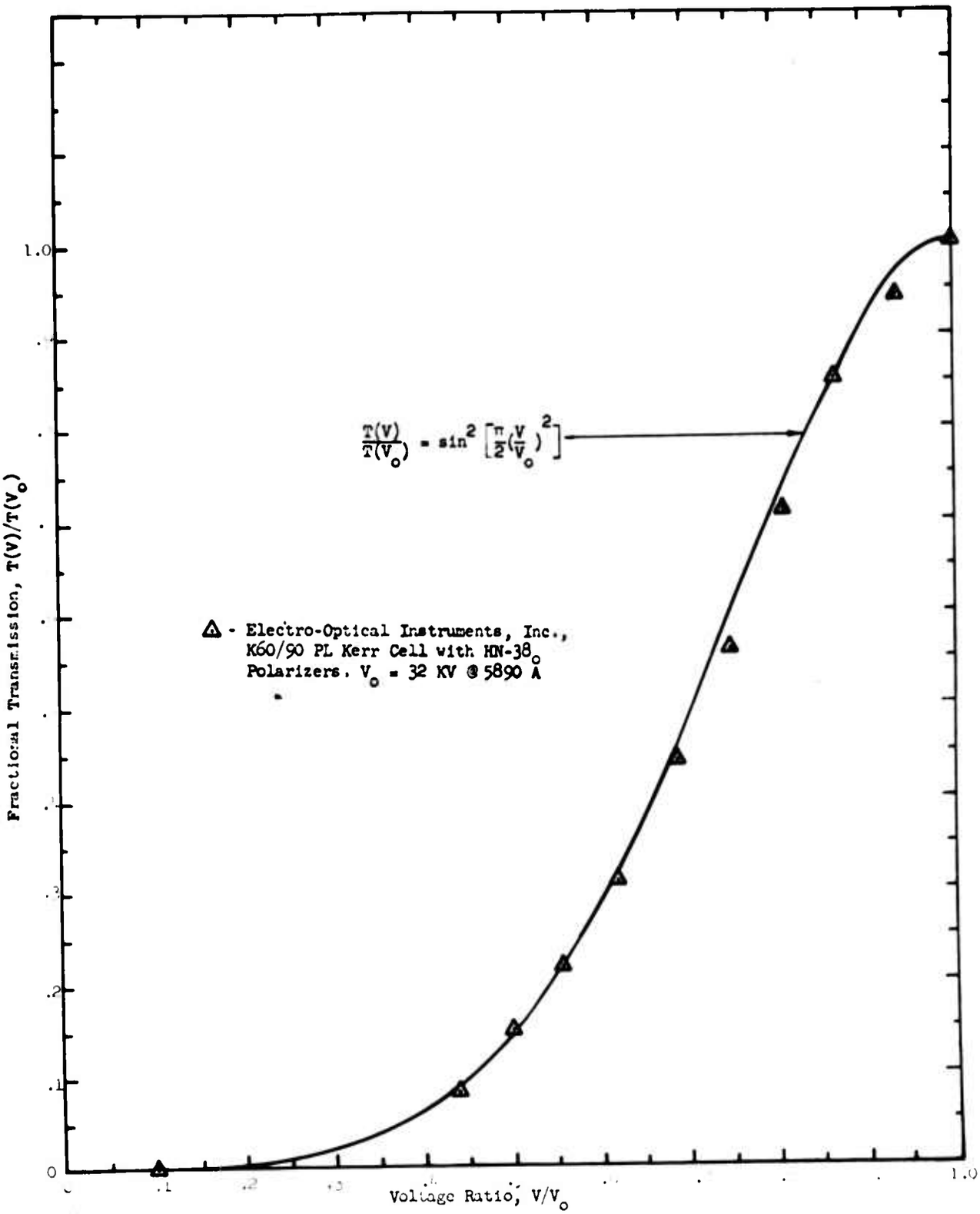

Fig. VII-3. Kerr Cell Filter Fractional Transmission Versus Applied Voltage Ratio.

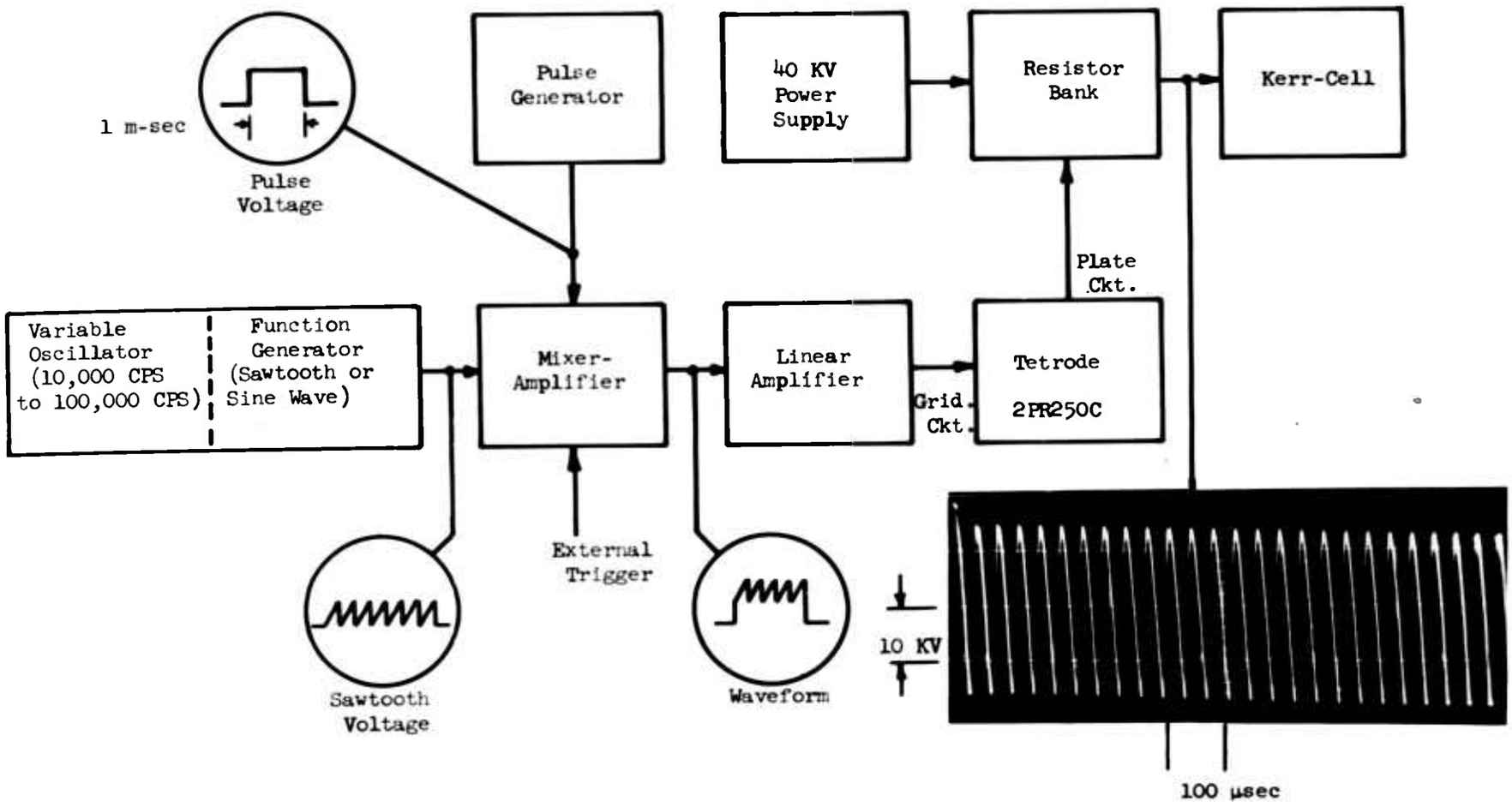

Fig. VII-4. Kerr-Cell Modulator Diagram

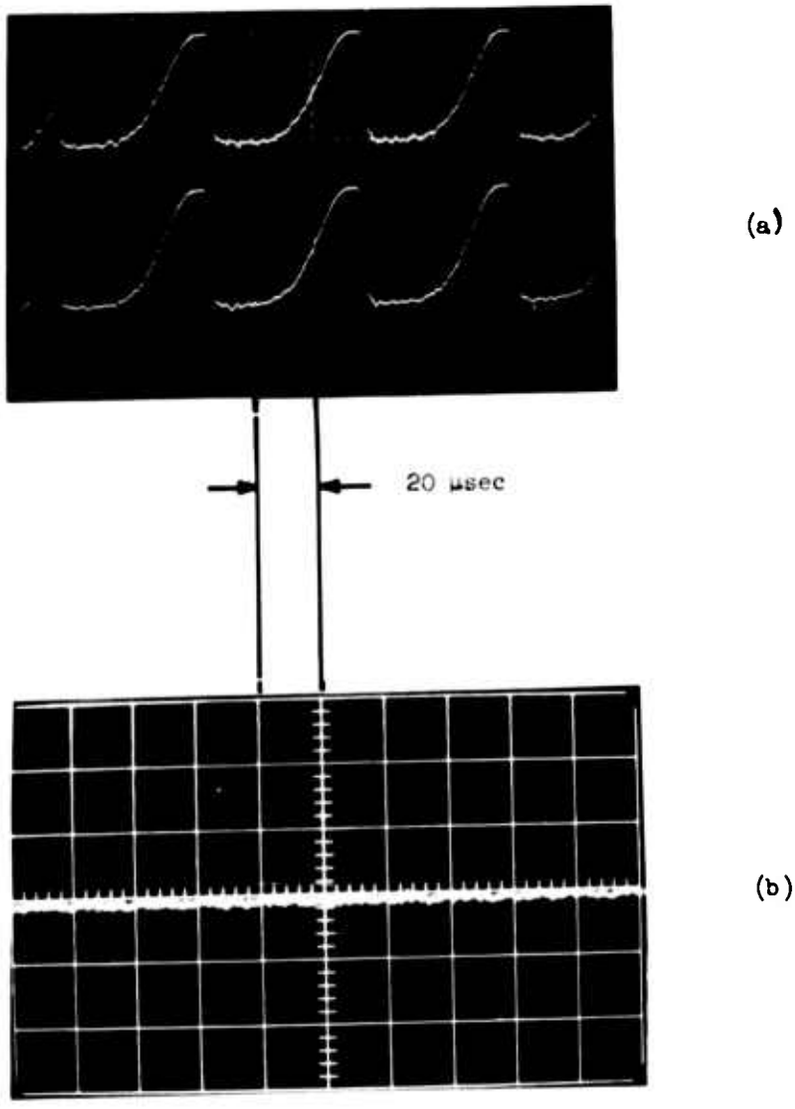

Fig. VII-5. (a) Oscilloscope traces of the photo-multiplier responses to the Kerr cell-modulated light source radiation. The upper trace corresponds to 5890 Å(λ_1) and the lower trace to 5880 Å (λ_2).
(b) Oscilloscope trace of the (a) signals differentially compared.

VIII. 8 MM LIGHT GAS GUN RANGE*

W. J. Hooker and E. J. Philbin

During the past twelve months, General Dynamics/Astronautics has been developing a light gas gun facility that could be used in conjunction with the wake temperature measurements[1,2] being made at the NASA Ames Research Center under the current Re-Entry Physics Research Contract. The basic launcher is now completed, and is shown in Fig. VIII-1.

The launcher is a deformable-piston light gas gun with an 8 mm launch tube. Loading conditions and performance curves are being prepared by the U. S. Naval Ordnance Laboratory, White Oak, Maryland, utilizing their hypervelocity launcher computer analysis.[3]

The test observation section is being made to accommodate the spectral line reversal temperature measuring apparatus currently used at Ames, a new multiple-pass Schlieren system for wake growth studies associated with the temperature measurements, and Abtronics image converter cameras for luminous wake pictures.

Initial test firings in this facility will be started in the month of June.

---

*Supported in total by General Dynamics/Astronautics, San Diego, California.

REFERENCES

VIII-1. Hooker, W. J., "Preliminary Hypervelocity Wake Brightness Temperature Measurements," General Dynamics/Astronautics, Space Science Laboratory Report No. GDA63-0506, October 1963.

VIII-2. Space Science Laboratory, "Re-Entry Physics Research Annual Report," General Dynamics/Astronautics, Space Science Laboratory Report No. GDA-DBE64-010, March 1964.

VIII-3. Piacesi, R. Gates, D. F., and Seigel, A. E., "Computer Analysis of Two-Stage Hypervelocity Model Launchers," U. S. Naval Ordnance Laboratory, White Oak, Maryland, Ballistics Research Report 67 (NOLTR62-87), August 1963.

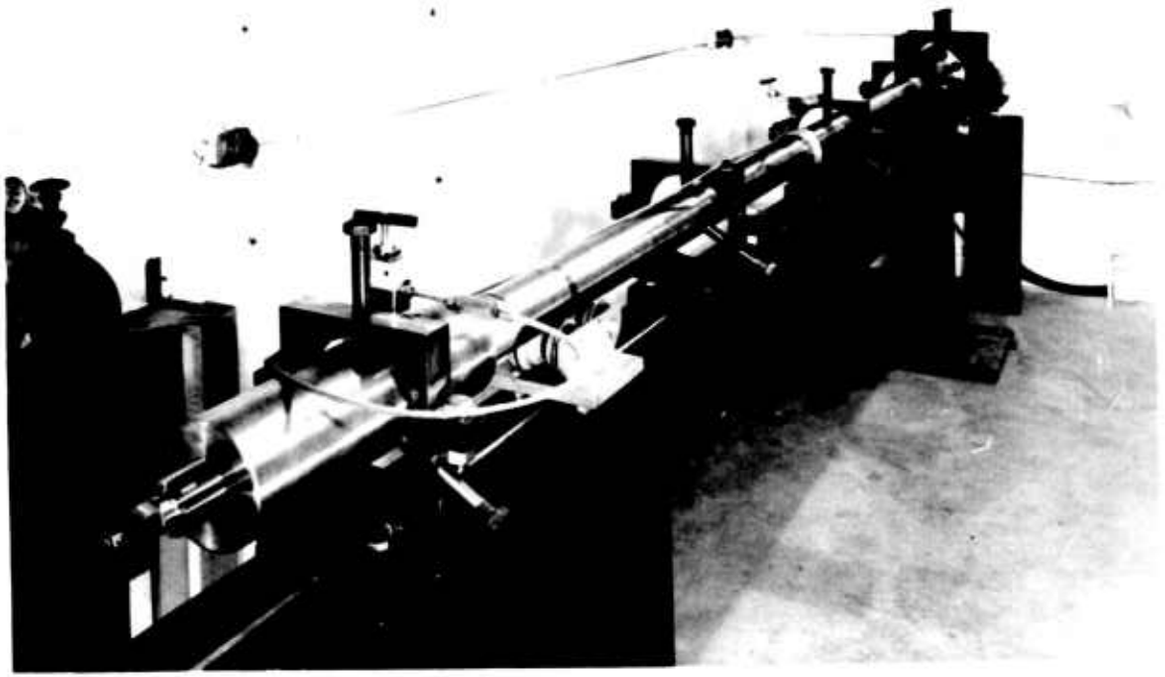

Fig. VIII-1. 8 mm Deformable - Piston, Light Gas Gun Launcher

IX. 24" SHOCK TUBE*

W. J. Hooker

During the past two years, General Dynamics/Astronautics has been developing a large shock tube facility that could be used in support of current Re-entry Physics Research projects, and which would allow us to look into new problem areas in the expanding field of chemical kinetics of contaminated wakes. The basic facility is now completed and is shown in Fig. IX-1.

The low pressure section has nominal dimensions of 24" diameter by 50' long, and is coupled to a 6" diameter driver by a 4' long conical transition section. The shock tube, for its initial measurements, will be cold-gas driven. However, a contract has been awarded to MHD Research, Inc., of Newport Beach, California, to perform a design study for an electrical driver for this shock tube.

The 24" shock tube was designed so that it could be used to study fast chemical reactions under conditions of low density and controlled high-purity. To this end, the shock tube, and associated pumping equipment, have been designed and fabricated to produce a high, uncontaminated vacuum in the test section.

The low pressure section of the shock tube was fabricated from 1/4" thick 304L stainless steel plates. The interior surfaces of the plates were ground and polished to a 4 microinch finish, and then covered with a

*Supported in total by General Dynamics/Astronautics, San Diego, California.

protective layer prior to subsequent rolling and welding operations. The assembled tube had all internal Heli-Arc welds ground and polished to blend into the surrounding surfaces.

Five pumping ports are equally spaced along the length of the tube. These ports are sealed by valve poppets that seat on a conical surface, and which are ground on the inside face to blend into the cylindrical shock tube surface. The ports have a nominal diameter of 7-1/2" and are retracted for pumping through a stroke of 10" by air-operated cylinders. The valve stems are sealed by Bel-Fab Corp. bellows to minimize air leakage during operation. When seated, the valve poppets blend uniformly into the tube wall. Sealing is accomplished with a Viton "O"-ring in the poppet conical surface.

The pumping ports lead to 7" Consolidated Vacuum Corp. PMC-1441 fractionating diffusion pumps, via liquid nitrogen cooled traps with full anti-creep barriers. The roughing operation in the 24" section is performed with a Consolidated Vacuum Corp. Heraeus-type 80 cfm mechanical pump through a 4" Vactite trap. The 6" driver section is evacuated through a re-entrant-type liquid nitrogen cooled trap by a Kinney KC8 mechanical pump. The five diffusion pumps are backed up by a fractional cfm mechanical pump during blank-off.

After having been brought up to atmosphere with trapped dry nitrogen, the 24" section can be evacuated to 100 microns Hg in 20 minutes. If the system has been well pumped prior to being brought up to atmosphere, the 5 diffusion pumps can place the 24" section into the 10^{-8} mmHg range, from 100 microns Hg, in less than 30 minutes. To date, the ultimate pressure in the tube is approximately 2-3 x 10^{-8} mmHg, while the blanked-off diffusion

pumps produce approximately 1×10^{-8} mmHg in the valve domes. At blank-off, the rate of total pressure rise in the 24" section is approximately 2×10^{-8} mmHg/min.

In order to analyze the composition of the residual gases in the 24" section, we have installed an Aero Vac Corp. Model AVAI Vacuum Analyzer in the transition section. The nude mass spectrometer analyzer tube is exposed to the high vacuum through a 2" gate valve, which is closed to protect the elements when the shock tube is fired.

A typical mass spectra is shown in Fig. IX-2. In this run, room air was drawn through an Edwards controlled leak valve into the 24" section where the total pressure was 4.5×10^{-6} mmHg. There is no discernible evidence of high molecular weight gases from diffusion pump oil cracking or "O"-ring degassing.

In Fig. IX-3 is shown a mass spectra obtained when the 24" section had been completely sealed and pumped on for four hours and the total pressure is 2.5×10^{-8} mmHg. In this trace, we see that virtually all of the residual air has been removed, and that only H_2O, and its OH and H_2 fragmentation products, remains. It can be easily shown, by applying heat to the shock tube surface, that this H_2O is absorbed on the internal surfaces. If the 24" section is blanked-off, and the mass spectra is scanned during pressure buildup, it is observed that the rate of rise of H_2O concentration accounts for nearly all of the pressure increase. This, then, allows us to set a measurable lower limit to the contamination level of H_2O, which so strongly affects many of the reactions observed in shock tubes. While this contamination level can be reduced by surface heating, we have not yet given

serious consideration to this aspect.

Platinum thin-film heat gauges, mounted flush with the internal surface of the 24" section, have been made for shock velocity measurement. Shock front curvature will also be measured with heat gauges mounted radially in the flat end flange of the 24" section.

The test-gas handling system, when completed, will employ purification and analysis techniques that will be consistent with the capability of the basic 24" facility.

The 24" shock tube facility will be operational in the second half of calendar 1964.

Fig. IX-1. 24" Shock Tube

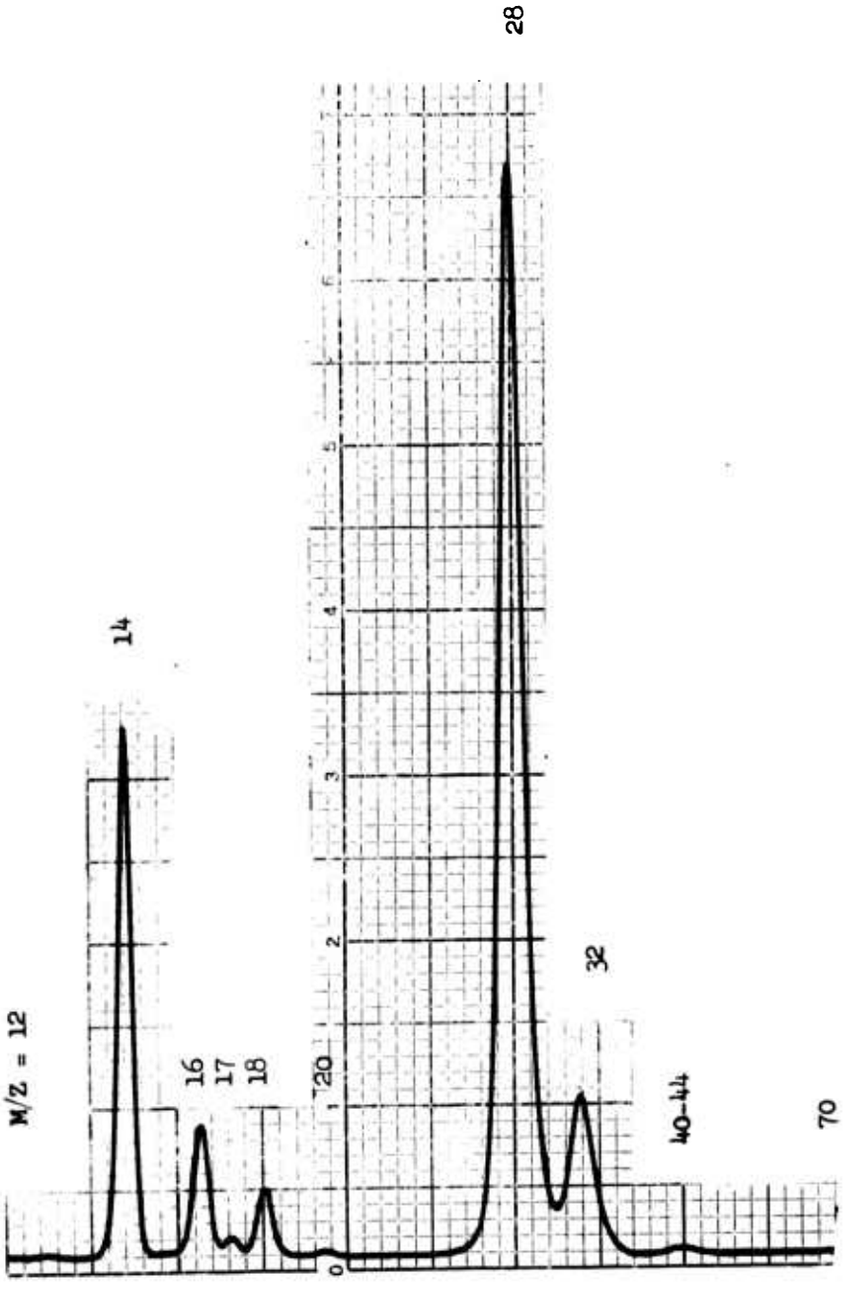

Fig. IX-2. Mass spectra obtained from an air leak into the 24" section. System pressure = 4.5×10^{-6} mmHg. M = mass number, Z = effective charge.

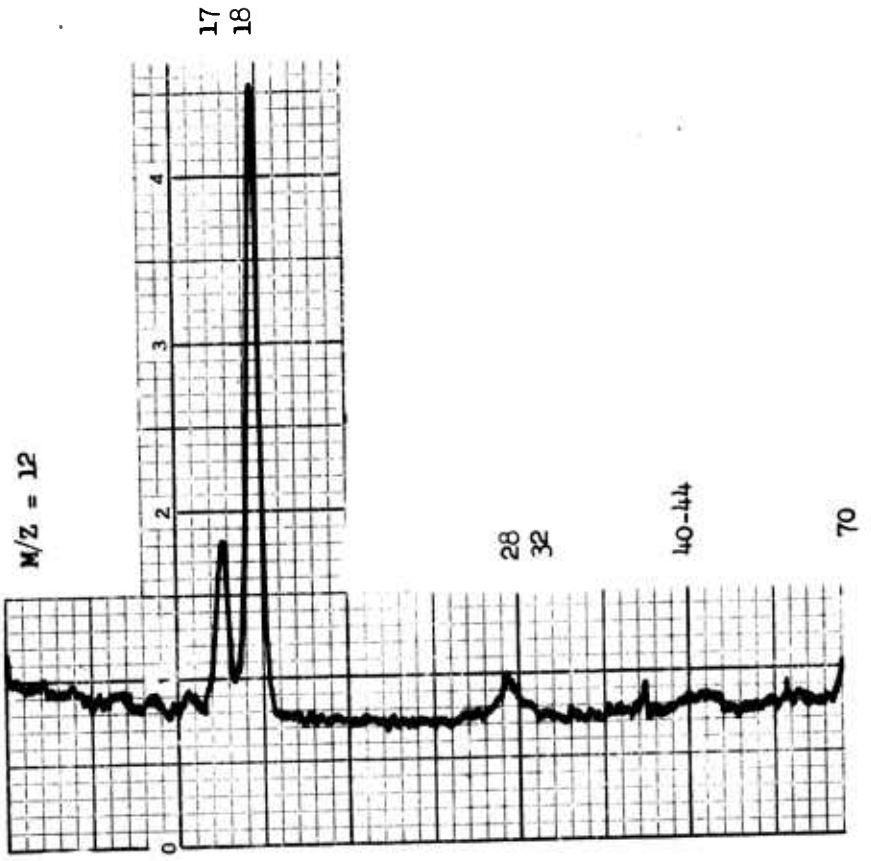

Fig. IX-3. Mass spectra obtained after 4 hours of pumping on the 24" section. System pressure = 2.5×10^{-8} mmHg. M = mass number, Z = effective charge.

UNCLASSIFIED